Journal of Volcanology and Geothermal Research 341 (2017) 104–118

Contents lists available at ScienceDirect

Journal of Volcanology and Geothermal Research

journal homepage: www.elsevier.com/locate/jvolgeores

Structural controls on fluid circulation at the Caviahue-Copahue Volcanic Complex (CCVC) geothermal area (Chile-Argentina), revealed by soil CO_2 and temperature, self-potential, and helium isotopes

Emilie Roulleau [a,b,c,*], Francisco Bravo [b], Daniele L. Pinti [d], Stéphanie Barde-Cabusson [c], Marcela Pizarro [a,b], Daniele Tardani [a,b], Carlos Muñoz [b], Juan Sanchez [b], Yuji Sano [e], Naoto Takahata [e], Federico de la Cal [f], Carlos Esteban [f], Diego Morata [a,b]

[a] Centro de Excelencia en Geotermia de las Andes (CEGA), Universidad de Chile, Plaza Ercilla 803, Santiago, Chile
[b] Departamento de Geología, Universidad de Chile, Plaza Ercilla 803, Santiago, Chile
[c] Laboratoire Magmas et Volcans – CNRS - IRD, OPGC, Université Clermont-Auvergne, Campus Universitaire des Cézeaux, 6 Avenue Blaise Pascal, 63178 Aubière Cedex, France
[d] GEOTOP & Département des sciences de la Terre et de l'atmosphère, Université du Québec à Montréal, Succ. Centre-Ville, CP8888, Montréal, QC H3C 3P8, Canada
[e] The University of Tokyo, Atmosphere and Ocean Research Institute, Kashiwa 277-8564, Japan
[f] Centro Administrativo Ministerial, Antártida Argentina 1245 - Edificio 4 - Piso 3, Neuquén, Argentina

ARTICLE INFO

Article history:
Received 16 January 2017
Received in revised form 10 May 2017
Accepted 12 May 2017
Available online 19 May 2017

ABSTRACT

Natural geothermal systems are limited areas characterized by anomalously high heat flow caused by recent tectonic or magmatic activity. The heat source at depth is the result of the emplacement of magma bodies, controlled by the regional volcano-tectonic setting. In contrast, at a local scale a well-developed fault-fracture network favors the development of hydrothermal cells, and promotes the vertical advection of fluids and heat. The Southern Volcanic Zone (SVZ), straddling Chile and Argentina, has an important, yet unexplored and undeveloped geothermal potential. Studies on the lithological and tectonic controls of the hydrothermal circulation are therefore important for a correct assessment of the geothermal potential of the region. Here, new and dense self-potential (SP), soil CO_2 and temperature (T) measurements, and helium isotope data measured in fumaroles and thermal springs from the geothermal area located in the north-eastern flank of the Copahue volcanic edifice, within the Caviahue Caldera (the Caviahue-Copahue Volcanic Complex - CCVC) are presented. Our results allowed to the constraint of the structural origin of the active thermal areas and the understanding of the evolution of the geothermal system. NE-striking faults in the area, characterized by a combination of SP, CO_2, and T maxima and high $^3He/^4He$ ratios (up to 8.16 ± 0.21Ra, whereas atmospheric Ra is 1.382×10^{-6}), promote the formation of vertical permeability preferential pathways for fluid circulation. WNW-striking faults represent low-permeability pathways for hydrothermal fluid ascent, but promote infiltration of meteoric water at shallow depths, which dilute the hydrothermal input. The region is scattered with SP, CO_2, and T minima, representing self-sealed zones characterized by impermeable altered rocks at depth, which create local barriers for fluid ascent. The NE-striking faults seem to be associated with the upflowing zones of the geothermal system, where the boiling process produces a high vapor-dominated zone close to the surface, whereas the WNW-striking faults could act as a boundary of the Copahue geothermal area to the south.

1. Introduction

Geothermal activity results from the interaction between a heat source, fluid circulation, and permeable pathways, promoting convective heat transfer. In geothermal systems, fluid residence times may range from a few hundred years to more than 20,000 years (Arnórsson, 1995; Arnórsson et al., 2007; Sveinbjörnsdóttir et al., 2001; Birkle et al., 2016), and are strongly controlled by the regional stress field and the local fault-fracture network. The main parameters of geothermal conceptual models are therefore the permeability architecture and the fluid geochemistry (Goff and Janik, 2000). The permeability architecture in geothermal areas is characterized by the geometry and the kinematics of the fault-fracture network (Sibson, 1996; Rowland and Simmons, 2012). This latter component may act as an impermeable barrier or as a high-permeability pathway, given that the permeability of faults and fractures depends on the host rock

* Corresponding author at: Laboratoire Magmas et Volcans- CNRS- IRD- OPGC, Université Clermont-Auvergne, Campus Universitaire des Cézeaux, 6 Av. Blaise Pascal, 63178 Aubière Cedex, France.
E-mail address: emilie.vinet-roulleau@uca.fr (E. Roulleau).

http://dx.doi.org/10.1016/j.jvolgeores.2017.05.010
0377-0273/

lithology and hydrothermal sublimate precipitation (Wibberley et al., 2008). Continuous hydrothermal mineral precipitation may seal intrinsic permeability related to both rock porosity (primary permeability) and open fracture networks (secondary permeability; Cox, 2010).

The Andean volcanic arc of Chile is one of the largest undeveloped geothermal provinces of the world, with an estimated potential of ~ 16,000 MW for at least 50 years of full production (Lahsen, 1988; Aravena et al., 2016). In Chile, geothermal resources occur in close spatial proximity to active volcanism along the Andean Cordillera, caused by the convergence of the Nazca and the South America Plates (Lahsen, 1988; Parada et al., 2007; Stern et al., 2007). Although there is consensus that volcanism and geothermal activity are largely controlled by the regional-scale tectonic stress field in the Southern Volcanic Zone (SVZ) (Alam et al., 2010; Hauser, 1997; Lahsen, 1988; Sanchez et al., 2013; Sepúlveda et al., 2005; Tardani et al., 2016), information is still lacking on how the local fracture-fault network controls the evolution of geothermal systems and drives fluid circulation.

The Caviahue-Copahue Volcanic Complex (CCVC) provides one of the best natural laboratories in which to assess the interplay of the fault-fracture network and the chemical evolution of geothermal systems at a local scale. This area includes the active Copahue volcano and an extended geothermal area on its NE flank, characterized by many superficial emissions (fumaroles, bubbling pools, thermal springs) spatially controlled by local faults (Nakanishi et al., 1995; Melnick et al., 2006). The recent work of Chiodini et al. (2015) presents the first CO_2 flux and soil temperature measurements in the geothermal area in order to define the total budget of hydrothermal gases released at the surface and estimate the minimum geothermal potential of this geothermal system. Thus, they provide the first CO_2 flux estimation of 165 t d^{-1} and the natural thermal release of 107 MW from the geothermal system of that sector of the CCVC. To explain the presence of this geothermal system, the authors suggest the presence of an active magmatic intrusion beneath this portion of the Caviahue caldera. Here, we aim to understand the relationship between geochemical variations and the fault network in the CCVC geothermal area based on dense self-potential (SP), soil CO_2 and temperature (T) profiles, and helium isotope ($^3He/^4He$) measurements of fumaroles and thermal springs. The role of NE- and WNW-striking structures in controlling the surface geothermal manifestations in the CCVC is highlighted, and a new interpretation of the fluid circulation in this geothermal system is proposed.

2. Study site

2.1. Tectonic setting

The Southern Volcanic Zone (SVZ), straddling Chile and Argentina, between 33°S and 46°S, is one of the four active arc segments of the Andes. Active volcanism along this segment (Fig. 1) is primarily controlled by the convergence of the Nazca and the South America Plates (Lahsen, 1988; Parada et al., 2007; Stern et al., 2007). Between 39°S and 46°S, geothermal and volcanic activity are partially controlled by the 1000 km long NNE Liquiñe-Ofqui Fault System (LOFS). This intra-arc dextral strike-slip fault system was generated as a consequence of the strain partitioning produced by the oblique subduction of the Nazca plate beneath the South American plate (Fig. 1). The LOFS is associated with second-order intra-arc anisotropy, having a dominant NE-SW and NW-SE orientation (Cembrano et al., 1992; Cembrano et al., 1996; Cembrano et al., 2000; Cembrano and Lara, 2009).

The CCVC is located in the Southern Andean Volcanic Zone (SAVZ; 37.5°S, 71°W), at the border between Argentina and Chile. It is composed of the Caviahue caldera and the Copahue stratovolcano (Fig. 1). Structurally, the CCVC is located in the accommodation zone of the northern part of the LOFS. The Caviahue caldera is a square-shaped depression (20 × 15 km) of Pliocenic age, and is defined as a transitional pull-apart, intra-arc basin due to the local stress field generated by the interaction of the LOFS and the reverse Copahue-Antiñir Fault System (CAFS; Melnick et al., 2006).

2.2. Volcanic and hydrothermal activity

The history of Caviahue caldera began 3–4 Ma ago, with the formation of the Caviahue caldera pull-apart structure (Melnick et al., 2006). The walls and the basement of the Caviahue caldera are basaltic and andesitic lavas, volcanic breccia, and minor sedimentary beds of the Cola

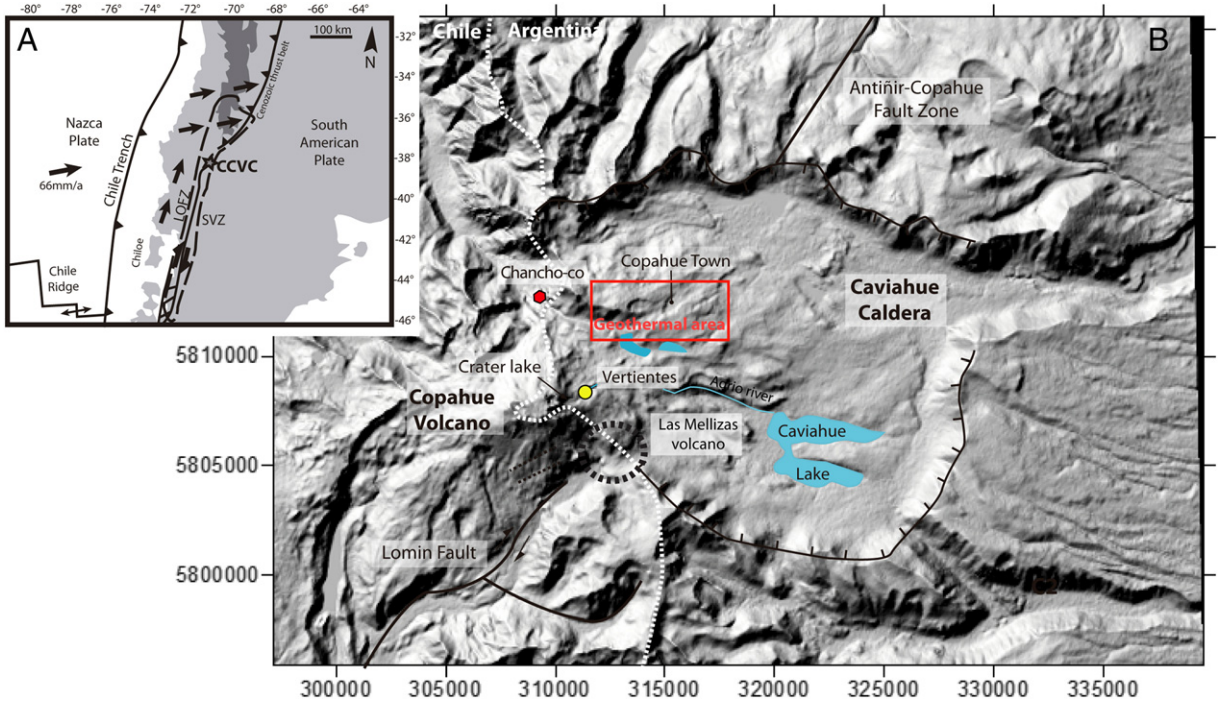

Fig. 1. Map of the Caviahue–Copahue Volcanic Complex (CCVC) showing the main structural features (map coordinates in m, UTM-WGS84 19S). LOFS: Liquiñe-Ofqui Fault System; SVZ: South Volcanic Zone.

de Zorro Formation (5–6 Ma; Linares et al., 1999), outcropping extensively in the main Cordillera, between 36°S and 39°S. Las Mellizas volcano (Fig. 1), located on the rim of the CCVC caldera, SE of Copahue volcano, is composed by three sequences: lower lavas, ignimbrites, and upper lavas. The ignimbrites are associated with the collapse of the Las Mellizas stratovolcano (Melnick et al., 2006), dated by K/Ar at 3.2 ± 0.14 Ma and 2.6 ± 0.1 Ma (Linares et al., 1999).

The Copahue volcano is an active andesitic to basalt–andesitic stratovolcano, nested on the western rim of the Caviahue caldera. Volcanic activity began approximately 1 Ma ago. Since the Upper Pleistocene, activity has consisted mainly of effusive emissions of andesitic lava flows and only a few explosive episodes during the Holocene, which generated at least six ash-flows (Linares et al., 1999; Muñoz and Stern, 1988). Over the last 250 years, Copahue volcanic activity was characterized by weak phreatic and phreatomagmatic eruptions. Copahue volcano has an acidic crater lake at the summit (pH ~0.2–1.1; Varekamp et al., 2009), characterized by intense magmatic degassing (Tamburello et al., 2015), and acidic hot springs (pH ~0.3–2.4), called Vertientes, near the summit that feed the Agrio River (pH ~0.5–2.5; Fig. 1). This river discharges into a large and acidified (pH: 2.1–2.7) glacial lake, called Lake Caviahue (Agusto, 2011; Caselli et al., 2005; Varekamp et al., 2001; Varekamp et al., 2009).

An extensive geothermal system is located inside the Caviahue caldera, spatially associated with the active Copahue volcano. The surface gas and water emissions are closely associated with NE- and WNW-striking faults (Nakanishi et al., 1995; Melnick et al., 2006). Five geothermal areas are recognized on the slopes of Copahue volcano, with surface manifestations including boiling and bubbling pools with temperatures reaching 96 °C, and fumaroles with temperatures of up to 135 °C (Agusto et al., 2007). Four of these, known as Las Maquinas, Las Maquinitas, Termas Copahue, and Anfiteatro thermal areas, are located northeast of the volcanic edifice, and appear to be related by a set of NE-striking faults (Melnick et al., 2006). The Chancho-có geothermal area is located on the northern flank of the Copahue volcano, in close proximity to the volcanic–hydrothermal system (Velez et al., 2011), and is controlled by a WNW-striking fault (Melnick et al., 2006). The composition of the bubbling gas emissions and the dry gas phase of the fumaroles from the studied geothermal area and the well gas (COP-2) are dominated by CO_2 (826,200 ppm to 970,450 ppm; Roulleau et al., 2016). The acidic gas species, HCl and HF, are present in low amounts (Roulleau et al., 2016). However, Anfiteatro gases show lower amounts of CO_2 and higher N_2 and He than Las Maquinas, Las Maquinitas, and Termas Copahue gases, suggesting a significant meteoric water interaction and crustal contamination probably at shallow depths (Roulleau et al., 2016). Significant concentrations of S_{total}, N_2, H_2, and CH_4 (59,069 ppm, 54,300 ppm, 14,553 ppm, and 44,408 ppm respectively; Roulleau et al., 2016) were detected. During geothermal exploration at the CCVC, a vapor-dominated hydrothermal system, composed of two different productive reservoirs, was recognized northeast of Copahue volcano. The reservoirs are located at 800–1000 m and 1400 m depths, and are characterized by temperatures estimated at 200 °C and 250–300 °C respectively (Agusto et al., 2013). The geothermal field of Copahue is composed of stratified layers developed in the Las Mellizas sequence (andesitic lava and ignimbrites), connected by fractures with increased vertical permeability.

3. Methods

Coupled measurements of CO_2 soil gas concentration and flux, soil temperature (T), and self-potential (SP) were carried out during a field campaign in March 2015, along six profiles for a total of ~13 km (Fig. 2).

3.1. Soil CO_2 concentration

On active volcanoes, CO_2 anomalies are generally associated with highly permeable zones, which may also drain heat and other fluids (Kerrick et al., 1995). 445 soil CO_2 concentration measurements were carried out with a 40 m spacing, doubling the measurement density (i.e., measurements taken every 20 m) in areas where shallow geothermal emissions were detected. The soil CO_2 concentration was obtained by pumping the gas through a 4 mm diameter copper tube inserted into the soil to a depth of ~30 cm; the CO_2 concentration is determined as the difference in potential provided by a calibrated GasCheck infrared gas sensor (from Edinburgh Sensors®). Two GasChecks with different concentration sensitivities (0–3000 ppm and 0–10% by volume) were used to avoid dilution issues. The accuracy of the CO_2 concentration measurements was ±3% for both gas check 3000 ppm and gas check 10%.

3.2. Soil CO_2 flux

185 soil CO_2 flux measurements were carried out, mainly in the area of geothermal manifestations. Measurements were done every 20 m, following the accumulation chamber method of Chiodini et al. (1998). The instrumentation consisted of an infrared (IR) spectrometer (LICOR-820) with a 0–20,000 ppm range. The accuracy of measured CO_2 fluxes is estimated to be 15%, including the variation in CO_2 flux at a given site. Statistical parameters for CO_2 flux measurements are presented in Table 1.

3.3. Soil temperature

281 soil temperature (T) measurements were carried out at a 20 m spacing in areas where superficial geothermal manifestations were present, and every 40 m elsewhere.

The probes were inserted into the soil to a depth of ~30 cm, and the temperature reading was taken using a digital thermometer after 15 min, the time needed to reach thermal equilibrium (Revil et al., 2008). Temperature anomalies are related to the shallow geothermal system associated with the active Copahue volcano. In the absence of vapor emission at the surface, the increase in soil temperature could be related to the condensation of water steam at depth, which releases large quantities of heat. The accuracy of temperature measurements is ±3%.

3.4. Self-potential

638 self-potential (SP) measurements were acquired every 20 m on each profile. A pair of $Cu/CuSO_4$ non-polarizing electrodes and a 300 m-long insulated electric cable were used. This method consists of measuring the natural difference in electrical potential between two points directly at the ground surface. The difference in electric potential between the reference electrode and the moving electrode was measured using a high-impedance voltmeter, the Extech EX520True-RMS Industrial Multimeter. The electric contact with the ground was usually less than 200 kΩ in active geothermal areas, since moisture was always found a few centimeters below the surface. SP values associated with a resistance of greater than 500 kΩ were excluded. Outside active geothermal areas, the electric contact with the ground gave higher resistance values, resulting in high background noise. Even in such cases, the signal was consistently stable, and values of greater than 1 MΩ were excluded. The typical offset error between the two electrodes was less than 5 mV. To avoid increasing this offset along the entire profile, the moving electrode and the reference electrode were switched for the next set of measurements and the loop closure computed.

SP anomalies in geothermal areas depend mainly on two mechanisms: electrokinetic and thermoelectric coupling, the first being significantly larger than the second (Corwin and Hoover, 1979). Electrokinetic potential is created by fluid flow in porous systems. In the absence of a geothermal system, fluid flow is restricted to the downward flow of vadose water to the water table. The presence of hydrothermal or geothermal areas produces positive SP anomalies (e.g.: Aubert,

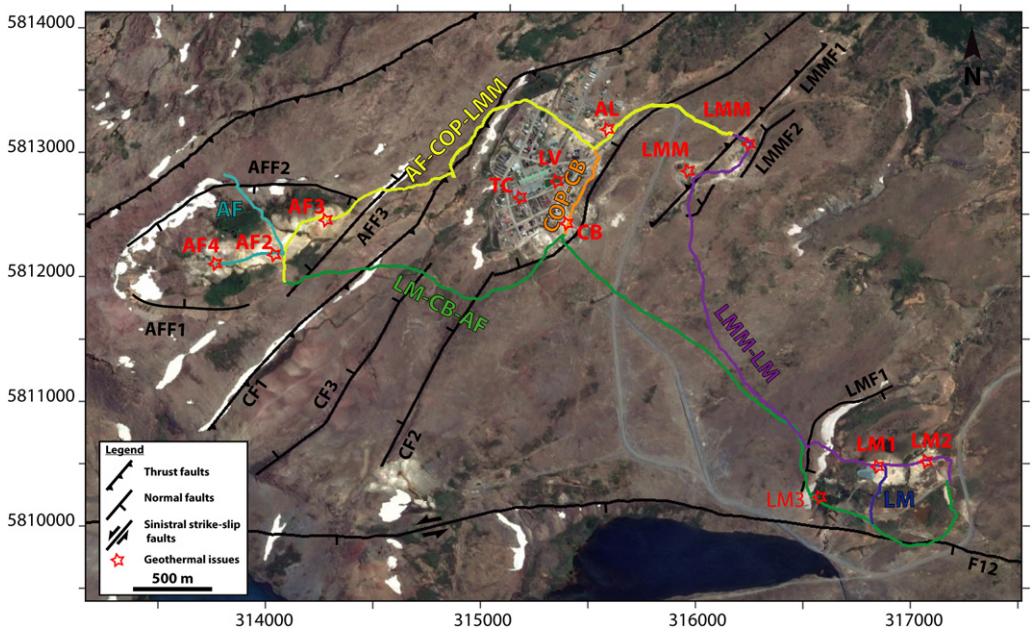

Fig. 2. Location of the six profiles (continuous colored lines) along which SP, soil CO_2, and T measurements were carried out, overlaying a satellite image of the CCVC geothermal area (map coordinates in m, UTM-WGS84 19S). The locations of the six profiles are indicated with different colors: Anfiteatro - Copahue Twon - Las Maquinitas (AF-COP-LMM) in yellow, Las Maquinitas - Las Maquinas (LMM-LM) in purple, Las Maquinas – Cabañita - Anfiteatro (LM-CB-AF) in green, Anfiteatro (AF) in blue, Copahue Twon - Cabanita (COP-CB) in orange and Las Maquinas (LM) in dark blue. Red stars represent the main geothermal sites where sample fluids were collected; AF-2-3-4: Anfiteatro, CB: Cabañita, LMM1-3: Las Maquinitas, LM1-2-3: Las Maquinas, Al, TC and LV: Copahue Town, and COP: Copahue well (Table 1). Black lines represent fault structures.

1999; Corwin and Hoover, 1979). However, an ambiguity may alter the interpretation of SP maxima. If the system is purely hydrogeological (i.e., no connection to the hydrothermal system), a SP maximum can occur in the case of a rise of the water table. Conversely, in a hydrothermal area, a SP maximum will correspond to the convective upward flow of fluids. This ambiguity can be resolved by coupling SP measurements with temperature and CO_2 measurements.

Because of the noisy background, SP results were not considered a priority in our discussion with respect to CO_2 concentration/flux, temperature, and He isotope data. However, the observed SP anomalies were used to support the geochemical data.

3.5. Helium isotopes

Thirteen gas samples were collected from Anfiteatro (AF2, AF3, and AF4), Banos Copahue (LV and TC), Agua Limon (AL), Cabañita (CB), Las Maquinitas (LMM1 and LMM3), Las Maquinas (LM1, LM2, LM3), and COP-2 (well) between January 2015 and January 2016 (Fig. 2 and Table 2). Sampling methods used for this part of the study are described in Roulleau et al. (2016).

The $^3He/^4He$ ratio (reported as R/R_A ratio: R = sample $^3He/^4He$, R_A = air $^3He/^4He$) was measured with a GV Helix-SFT® noble gas mass spectrometer at AORI-University of Tokyo (Japan), and using a Thermo Helix MC Plus® multi-collection noble gas mass spectrometer at GEOTOP (Montréal, Canada). The $^4He/^{20}Ne$ ratio was measured at AORI using an online quadrupole mass spectrometer. Helium was separated from Ne using a cryogenic trap held at 40 K (Sano and Wakita, 1988). Measured $^3He/^4He$ ratios were calibrated against atmospheric helium. Experimental errors for $^4He/^{20}Ne$ and $^3He/^4He$ ratios were approximately 5% and 1% at 1σ (Sano et al., 2008). Please refer to Roulleau et al. (2015b) for additional information on the AORI facility.

Helium isotopic ratios ($^3He/^4He$) for the 2016 survey samples were measured at the Noble Gas Laboratory of GEOTOP. See Roulleau et al. (2013) for details on noble gas analyses using the quadrupole mass spectrometer at GEOTOP.

The $^3He/^4He$ ratio was corrected for air contamination using the $^4He/^{20}Ne$ ratio measured in the sample (Craig et al., 1978). The corrected $^3He/^4He$ ratios (Rc), normalized to that of the atmosphere ($Ra = 1.382 \times 10^{-6}$; Sano et al., 2013), were within 1% of the measured value.

4. Results and interpretation

4.1. General results for the geothermal area

The results of soil CO_2 concentration and flux, T, and SP measurements are given for AF-COP-LMM (Fig. 3), LMM-LM (Fig. 4), LM-CB-AF (Fig. 5), AF (Fig. 6), LM (Fig. 7), and COP-CB (Fig. 8). The $^3He/^4He$ ratios normalized to the atmospheric ratio ($Ra = 1.382 \times 10^{-6}$; Sano et al., 2013), Rc/Ra, are presented together with $^4He/^{20}Ne$ ratios in Table 2.

Given the low variation in elevation in the study area (less than 165 m), the elevation parameter does not substantially influence the

Table 1
Statistic parameters for CO_2 flux and concentration, temperature and self-potential data.

	CO_2 flux	CO_2 concentration	Temperature	Self-Potential
Average	112.25 (g m^{-2} d^{-1})	10,092 (ppm)	24.00 (°C)	54 (mV)
Std deviation	291.77	45,154.32	17.11	56.60
Minima	0.05 (g m^{-2} d^{-1})	371 (ppm)	11.1 (°C)	−332 (mV)
Maxima	1709.60 (g m^{-2} d^{-1})	591,969 (ppm)	88.9 (°C)	368 (mV)
Measurements	185	445	281	638
Amount of used data	170	445	281	633

Table 2
He and Ne compositions for the geothermal fluids of CCVC.

Samples	Dates	Location	Longitude –E	Latitude -S	Type of emission	Temp. (°C)	$^4He/^{20}Ne$	R/Ra	±	Rc/Ra	±
AF2	2015	Anfiteatro[a]	314094	5812540	Fumarole	92.3	58.0	5.11	0.05	5.13	0.05
AF3	2016	Anfiteatro	314279	5812390	Bubbling gas	85.5	56.6	7.14	0.20	7.17	0.20
AF4	2016	Anfiteatro	313708	5812321	Bubbling gas	65.4	38.7	4.61	0.10	4.64	0.10
COP-2	2015	COP-2[a]	314918	5811238	Well	220	233.6	7.50	0.06	7.51	0.06
LM1	2015	Las Maquiñas[a]	316798	5810815	Fumarole	93	562.4	7.09	0.04	7.10	0.04
LM2	2015	Las Maquiñas[a]	317095	5810827	Bubbling gas	92.5	87.8	7.32	0.15	7.34	0.15
LM3	2016	Las Maquinas	316297	5810485	Bubbling gas	79.3	77.8	6.83	0.20	6.85	0.20
LMM1	2015	Las Maquiñitas[a]	316522	5812479	Bubbling gas	94.5	12.3	7.31	0.06	7.48	0.06
LMM3	2016	Las Maquinitas	316004	5812123	Bubbling gas	88.4	145.5	6.75	0.14	6.76	0.14
CB	2015	Cabañita[a]	315605	5812315	Fumarole	92	652.2	7.86	0.1	7.86	0.07
AL	2016	Agua limon	315928	5812757	Bubbling gas	84.7	15.5	8.01	0.21	8.16	0.2
TC	2016	Bano Copahue	315412	5812554	Bubbling gas	81.9	173.8	7.35	0.21	7.36	0.2
LV	2015	Baño Copahue[a]	315615	5812608	Bubbling gas	35.2	32.4	7.49	0.03	7.55	0.03

Note: the coordinates are expressed in m, UTM-WGS84 19S.
[a] Data from Roulleau et al. (2016).

SP variations (Sasai et al., 1997; Onizawa et al., 2009). CO_2 flux and concentration peaks in the south-east of the study area match the fumarolic and bubbling gas emanation of Las Maquinas (Figs. 4–5). High temperatures (up to 88 °C) and high Rc/Ra, close to that of the upper mantle (8 ± 1Ra), of between 6.85 ± 0.20 Ra (LM3) and 7.34 ± 0.15 Ra (LM2), are also associated with SP maxima.

High CO_2 flux and concentration peaks that also show high temperatures (up to 93 °C) and high Rc/Ra, ranging from 6.76 ± 0.14 Ra (LMM3) to 7.45 ± 0.06 Ra (LMM1), are observed in the fumarolic area of Las Maquinitas (Fig. 4). Small SP anomalies are observed in the two fumarolic areas of LMM1 and LMM3.

Copahue Town (Figs. 3–5 and 8) presents particularly high CO_2 flux and concentration values, mainly in the geothermal manifestation areas of Agua Limon (AL), Baño Copahue (LV and TC), and Cabañita (CB). In these three zones, high temperatures and Rc/Ra (88 °C and up to 8.16 ± 0.21 Ra respectively) correspond with small positive SP anomalies.

On the north flank of the Copahue volcano, Anfiteatro, which is delimited by two compressive WNW-striking faults, shows low CO_2 concentrations (up to 58,292 ppm; Figs. 3–6) compared to those at the village of Copahue (up to 414,995 ppm), which are consistent with the observed low fumarolic and bubbling gas emanations referred to as AF4 and AF2. Temperatures are not higher than 51 °C and Rc/Ra is usually lower than mantle values (4.63 ± 0.10 Ra and 5.12 ± 0.05 Ra). These results are consistent with the presence of meteoric water in the amphitheater structure and suggest an interaction between superficial water and bedrock (i.e., the addition of radiogenic ^4He produced from the decay of U and Th contained in local sediments; Roulleau et al., 2016). The 2016 sampling campaign in this sector revealed particularly high Rc/Ra values (7.17 ± 0.20 Ra at AF3), never observed before in the eastern border of Anfiteatro, and correlated with a moderate peak in CO_2 concentration (50,982 ppm to 58,292 ppm).

4.2. General results for the hydrogeological areas

In the hydrogeological areas, where no geothermal manifestations are observed, CO_2 concentrations are usually atmospheric (~400 ppm; NOAA data), and temperatures are close to the ambient temperature at the time of this campaign (~17 °C). The SP signal shows some minima interpreted as water infiltration along small fractures. The SP variations are also controlled by the water table elevation, as is clear for areas HG1 and HG2 (Figs. 4 and 5), as well as for areas HG3 to HG6 (Figs. 3 to 5). Usually, these changes in water table elevation are delimited by faults (CF, CF3, F8; see Figs. 3 to 5). On the western part of Las Maquinas, a small increase in CO_2 concentration (from 465 ppm to 1033 ppm) and an abrupt SP decrease, called L1 (Fig. 5), mark the change in lithology between the Upper Lava and Ignimbrite units. Finally, in the western part of Cabañita (Fig. 5), small positive CO_2 peaks (647 ppm to 1033 ppm) are observed along CF1 and CF2 faults, which suggest that the end of these main faults can still guide ascending fluids to the surface.

4.3. Results for detailed multi-method profiles

In this section, soil CO_2 concentration, diffusive soil CO_2 flux, self-potential and soil temperature, are presented in detail for each profile. A strong correlation between soil CO_2 concentration and CO_2 flux measurements is observed.

4.3.1. Profile AF-COP-LMM

Fig. 3 presents the Anfiteatro – Copahue Town – Las Maquinitas (AF-COP-LMM) profile of SW-NE orientation. The geothermal areas, Copahue and Anfiteatro, are limited by main NE- and WNW-trending faults respectively (Rojas Vera et al., 2009), suggesting that the geothermal areas are bounded by structural discontinuities (AFF1, AFF2, AFF3, CF1, and CF2; Fig. 3). It is worth noting that the main faults generally coincide with positive CO_2 and T peaks associated with a large SP peak, but not systematically. The large SP peak could be the result of the abrupt topographical break associated with the fault, and be dependent only on the depression shape that can channel meteoric water flow. This particular type of SP signal was observed in caldera-type and pit crater-type collapses that show this dependence of the SP signal on the depression pattern (Barde-Cabusson et al., 2009; Roche et al., 2000).

In Anfiteatro and Copahue Town, a succession of positive CO_2, T, and SP positive peaks (e.g. grey field from I to III; Fig. 3) from AFF1 to AFF3 (boundary of the Anfiteatro; Fig. 2) and from CF1 to CF2 could be considered a normal feature for hydrothermal zones (Aubert, 1999; Finizola et al., 2003; Matsushima et al., 1990). These positive peaks in CO_2, T, and SP reflect a series of hot spots, identifiable by the presence of a series of fumarole and bubbling gas spots. Between each positive CO_2, T, and SP peak (grey fields from I to VI; in Fig. 3) from Copahue and Anfiteatro, CO_2, T, and SP rapidly decrease to background levels. This hydrothermal area, characterized by a series of discrete small anomalies, could be interpreted as an almost entirely self-sealed zone (Finizola et al., 2003). In hydrothermal areas, precipitation of secondary minerals (including clay, silicates, sulfates, sulfides, carbonates, and (hydr)oxides) tends to decrease the permeability of the medium, a phenomenon known as "self-sealing" (Harris and Maciejewski, 2000; Zlotnicki, et al., 2009; Kiryukhin, 2013; Di Maio and Berrino, 2016). Altered rocks (observed in the field in each thermal area as clay alteration) can therefore behave as natural geological barriers (Barde-Cabusson et al., 2009; Revil et al., 2002), forming a sealed zone at depth, impermeable to gases and fluids. Secondary permeability thus takes over to promote hydrothermal fluid circulation in these altered zones.

In the Anfiteatro geothermal zone, a positive SP peak (268 mV to 368 mV) associated with absence of CO_2 and T peaks is also noted, referred to as OS1 (Fig. 3). This is an ambiguous situation, but could reflect

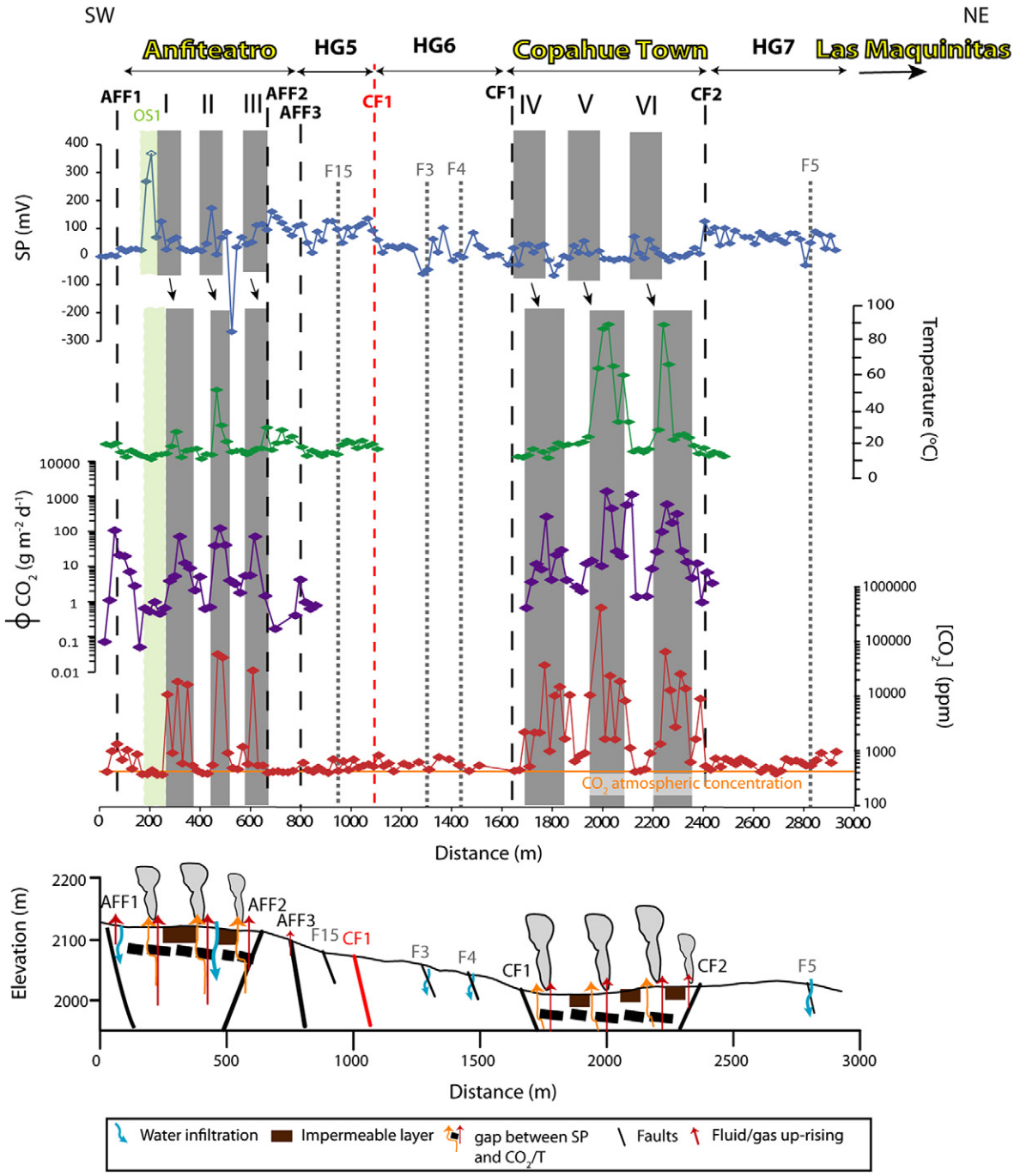

Fig. 3. Self-potential (SP), soil temperature, soil CO_2 flux, and soil CO_2 concentration along the Anfiteatro - Copahue Town - Las Maquinitas (AF-COP-LMM) profile. SP maxima and CO_2 and T peaks are numbered I, II, III, IV, V, VI: hydrothermal system from Copahue and Anfiteatro. The dotted lines represent the main and secondary faults. A schematic model in cross-section is presented with its topography. Hydrothermal activity is indicated by smoke symbols.

the presence of an old structural limit that is totally impermeable due to the precipitation of hydrothermal minerals, such as clay, chlorite, and calcite. This was also observed in the NW-trending faults by JICA (1992). The pH variation due to calcite precipitation can produce a reverse SP polarity (Guichet et al., 2006). Instead of a negative SP peak, which would be consistent with the absence of CO_2 and T peaks (as observed in the AF-COP-LMM profile), a positive SP peak is generated by the infiltration of water in contact with these precipitated hydrothermal minerals. The OS1 structure could therefore be defined as a preferential limit that allows water infiltration through hydrothermal calcite present at depth. During fieldwork, it was observed that Anfiteatro stores water, supporting the hypothesis of water exchange at shallow depth.

In the geothermal zones of both Copahue and Anfiteatro, a gap of 20 m between SP maxima and positive CO_2 and T peaks is noted. If the presence of a low permeability layer with a strong dip is considered (Finizola et al., 2003), it is possible to imagine that this layer could be impermeable to liquid phases, but not to a gaseous phase. The fluids would have to rise by buoyancy following the dip (Finizola et al., 2003), whereas the gases diffuse through this low permeability layer.

In the hydrogeological zones referred to as HG5 and HG6 (Fig. 3), fault CF1 separates two SP plateaus: a first one at ~100 mV and a second one at 0–20 mV. In both cases, the absence of CO_2 and T positive anomalies is noted. The break in the SP pattern observed in CF1 can be interpreted in terms of water table depth variation, supporting the

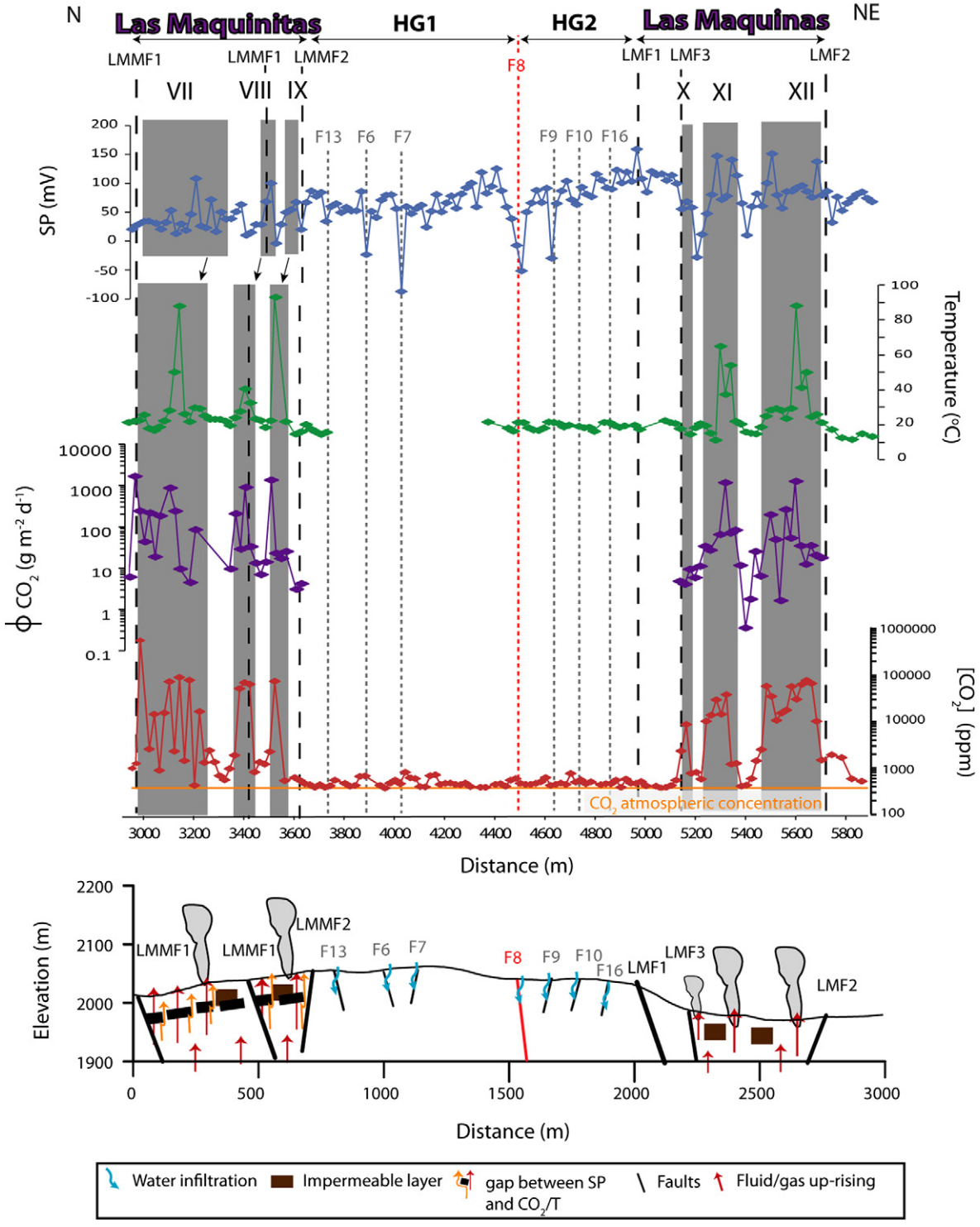

Fig. 4. Self-potential (SP), soil temperature, soil CO_2 flux, and soil CO_2 concentration along the Las Maquinitas - Las Maquinas (LMM-LM) profile. SP maxima and CO_2 and T peaks are numbered VII, VIII, IX, X, XI, XII: hydrothermal system from Las Maquinitas and Las Maquinas. The dotted lines represent the main and secondary faults. A schematic model in cross-section is presented with its topography. Hydrothermal activity is indicated by smoke symbols.

presence of two aquifers at different depths (Bennati et al., 2011; Finizola et al., 2004). Small negative SP peaks, referred to as F3, F4, and F5 are also observed, which could illustrate the presence of inferred secondary faults or fractures guiding water infiltration. These faults and fractures were observed in the field, oriented NE (F5) and NW (F3 and F4).

4.3.2. Profile LMM-LM

In proximity to both Las Maquinitas and Las Maquinas, the geothermal zone is delimited by NE-striking faults (LMMF1, LMMF2, LMF1, LMF2, and LMF3; Fig. 4) (Melnick et al., 2006; Rojas Vera et al., 2009); note that the measurement profile reaches LMMF1 twice. Usually, these faults are associated with positive CO_2 and T peaks, whether or

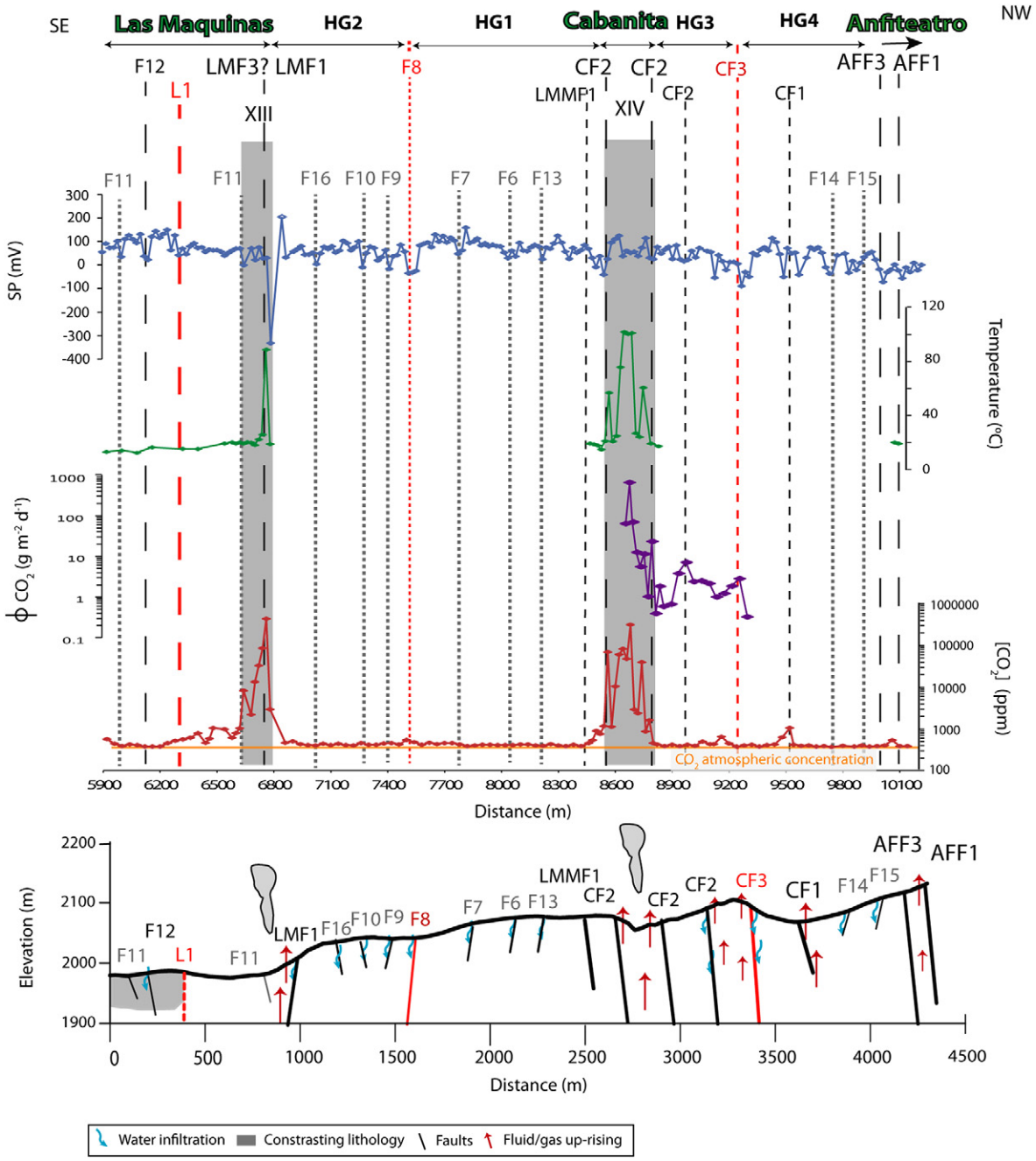

Fig. 5. Self-potential (SP), soil temperature, soil CO_2 flux, and soil CO_2 concentration along the Las Maquinas – Cabañita – Anfiteatro (LM-CB-AF) profile. SP maxima and CO_2 and T peaks are numbered XII, XIV: hydrothermal system from Cabañita and Las Maquinas. The dotted lines represent the main and secondary faults. L1 represents the lithological transition from upper lava to ignimbrites from Las Mellizas sequence. A schematic model of the structure is presented with its topography. Hydrothermal activity is indicated by smoke symbols.

not they are associated with a change in the SP signal. This signal clearly suggests the importance of the NE-trending fault in the uprising of geothermal fluids (JICA, 1992) in the study area.

The Las Maquinitas-Las Maquinas (LMM-LM) profile (Fig. 4) shows the same features as the AF-COP-LMM profile, as well as some peculiar additional features. In the hydrothermal areas of Las Maquinitas and Las Maquinas, CO_2, T, and SP maxima (grey field from VII to XII; Fig. 4) are interspersed by minima of the respective parameters. These minima may reflect the presence of altered rocks at depth that create an impermeable barrier to gases and fluids, as was observed in the AF-COP-LMM profile (Fig. 3). The minima at 5200 m along the profile (60 m wide) could be explained by freshwater infiltration. In the field, this area is characterized by the presence of wetlands and small lakes. The minima at 5400 m along the profile illustrates the boundary between two lithologies, namely the ignimbrite and the upper lavas from the Las Mellizas sequences (Melnick et al., 2006). This boundary behaves as a preferential pathway for the infiltration of meteoric or condensed water. In Las Maquinitas, a gap of 30 m between SP maxima and CO_2 and T maxima (grey field from VII to IX) is observed, and could be explained by a low permeability layer showing a strong dip, inducing the spatial separation of the liquid phase flowing up (ascent by buoyancy following the dip) and gases (Finizola et al., 2003).

In the hydrogeological zones referred to as HG1 and HG2, the fault F8 separates two SP plateaus: a first one ranging from 100 to 120 mV and a second one at ca. 70–80 mV (Fig. 4). It appears that this fault separates two aquifers located at two different depths. This can happen when a fault affects a preexisting aquifer guided by the lithology. While the fault displaces the stratigraphic layers vertically, it also creates a vertical

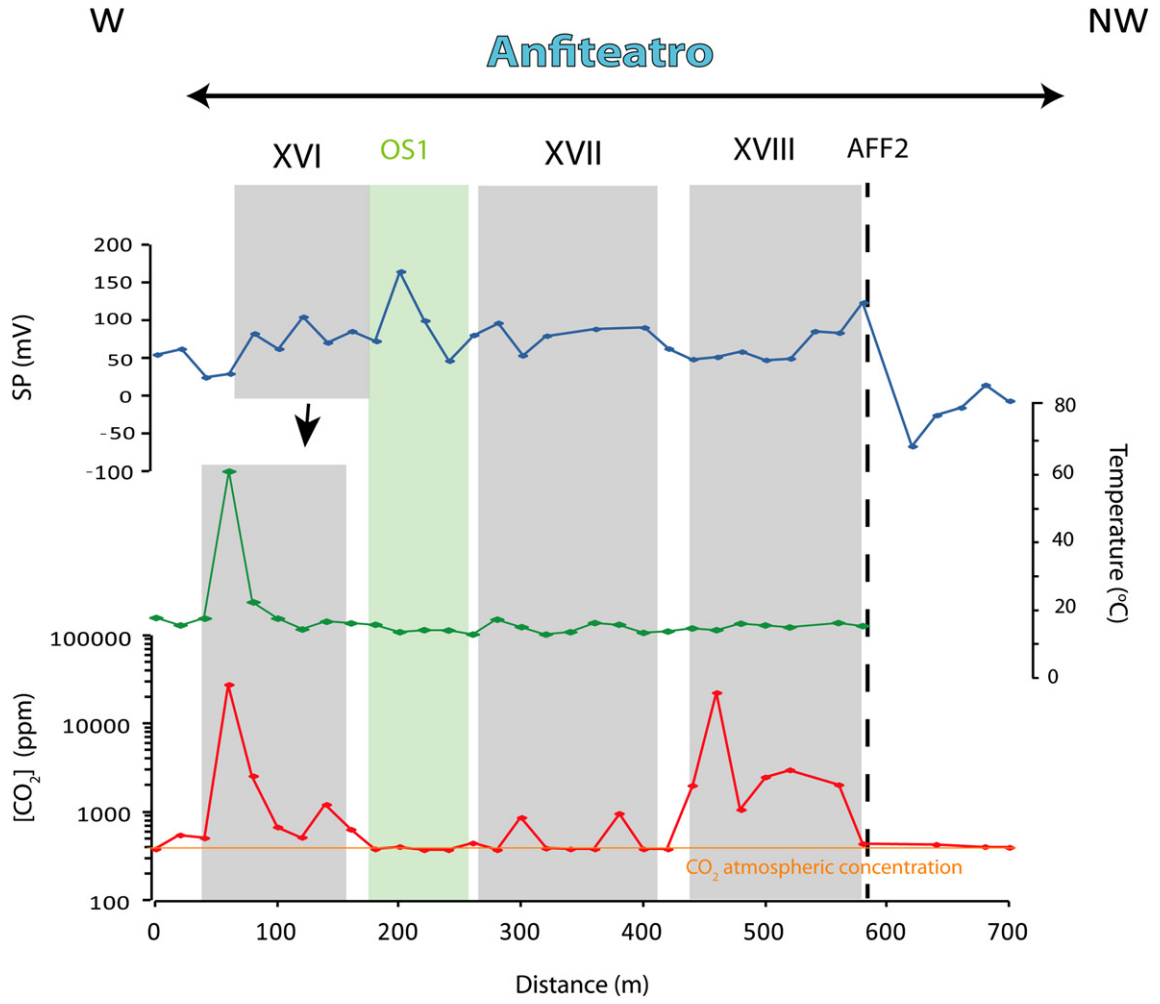

Fig. 6. Self-potential (SP), soil temperature, and soil CO_2 concentration along the Anfiteatro (AF) profile. SP maxima and CO_2 and T peaks are numbered XVI, XVII, XVIII: hydrothermal system from Anfiteatro. OS1 represents an old structure where calcite precipitation generates a pH modification and the reverse SP positive polarity, suggesting water infiltration. The dotted lines represent the main and secondary faults.

offset between the two parts of the aquifer on both sides of the fault (e.g., Bolós et al., 2014). The first plateau, between F7 and F8, shows a gradual increase in SP that could be related to the decrease in the vadose zone thickness (Aubert and Atangana, 1996; Bennati et al., 2011). This variation in unsaturated zone thickness is related to the topographical variation that decreases by ca. 20 m. Finally, a succession of SP minima (F13, F6, F7, F8, F9, F10, F16; Fig. 4), reaching values up to −100 m, is observed, and is evidence of secondary faults, with NE orientation as apparent in the field, permitting water infiltration.

4.3.3. Profile LM-CB-AF

Fig. 5 shows the Las Maquinas-Cabañita-Anfiteatro (LM-CB-AF) profile, where the Cabañita area has fumarole (CB) and bubbling gas emanations, which were active over the last 10 years. These two areas, Las Maquinas (referred to as XIII) and Cabañita (referred to as XIV), are defined as hydrothermal zones by the presence of CO_2, T, and SP maxima (Fig. 5). In Las Maquinas, the hydrothermal activity is delimited by two faults, F11 and LMF3 (note that F11 is crossed by the present profile twice). LMF3, oriented NE in the satellite image (also observed in LMM-LM profile; Fig. 4), is characterized by very strong positive CO_2 and T peaks, suggesting the ascent of gases without liquids (which are associated with negative SP peaks). F11, oriented NW according to our observations in the field, is characterized by a SP minimum and a CO_2 maximum. A similar structural setting was observed in Stromboli (Finizola et al., 2002), and suggests decreasing heat energy and upflow with depth, facilitating water infiltration. However, the presence of the CO_2 maximum could suggest that this fault is still able to guide gases to the surface. In the area of Las Maquinas, L1 separates two SP plateaus: a first one at 100-150 mV and a second one at 70–80 mV (Fig. 5). These two plateaus, as in previous profiles, could be explained by the presence of two aquifers at different depths. However, SP variation is associated with the increase in CO_2 concentrations and T, suggesting a permeability variation in this area. Melnick et al. (2006) demonstrated the presence of lithological variation in the Las Maquinas area, from the upper lava to the ignimbrite units of the Las Mellizas sequence. Thus, the first plateau most likely illustrates the impermeable upper lava unit, while the second represents the more permeable ignimbrite unit.

In Cabañita (central part of Fig. 5), T, CO_2, and SP maxima are limited by the main CF2 fault, oriented NE (Melnick et al., 2006; Rojas Vera et al., 2009), which is crossed three times by the profile (Fig. 5). CO_2 and T maxima, with SP minima, are observed in the Cabañita hydrothermal field (grey field referred to as XIV), suggesting the presence of a more impermeable layer that prevents the liquid phase from rising, but of sufficient permeability to enable the ascent of gases. In La Soufriere Volcano (Guadeloupe, France), a strongly altered dome was observed and characterized by a wide range of SP and resistivity values that reflected variations in water content and alteration level of the andesitic material constituting the volcano (Brothelande et al., 2014). Thus, in the case of the Cabañita area, it strongly suggests that altered rocks could produce ambiguous SP pattern due to the resulting permeability variation and to the precipitation of hydrothermal minerals, which may reverse the polarity of the SP anomalies (Barde-Cabusson et al., 2009; Revil et al.,

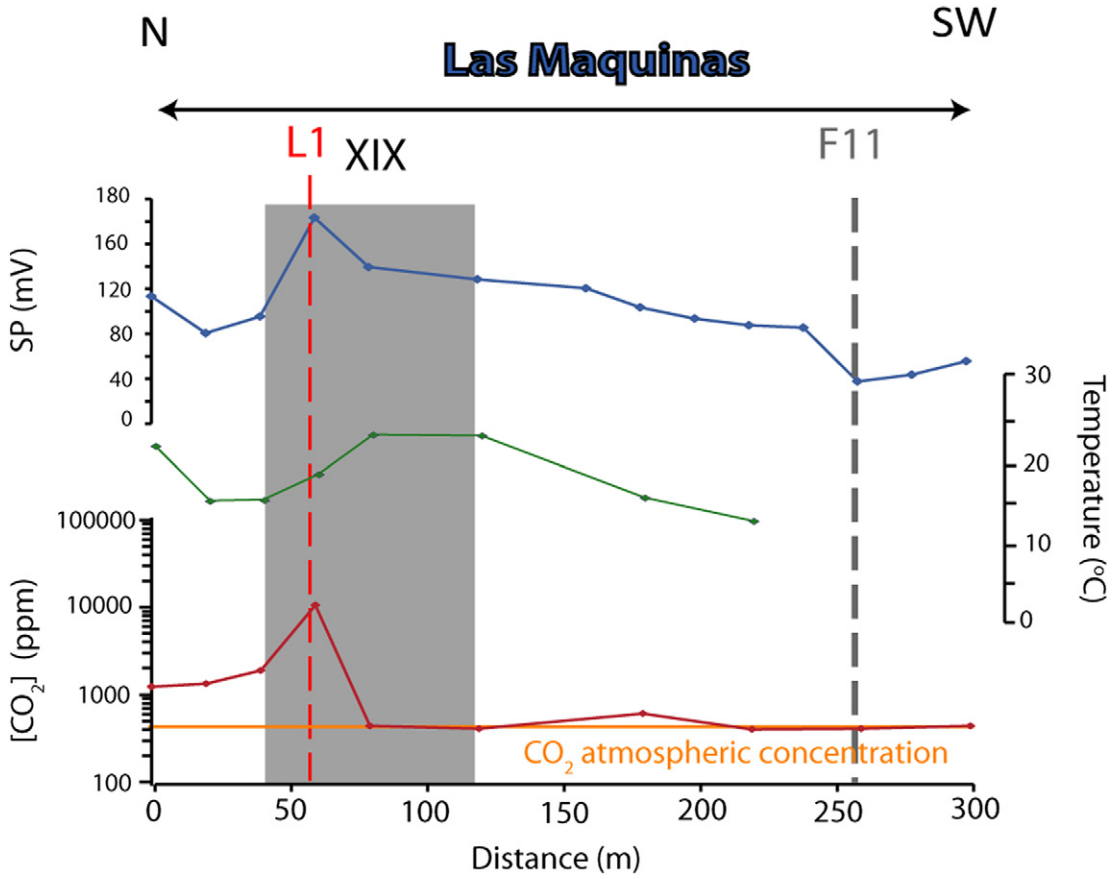

Fig. 7. Self-potential (SP), soil temperature, and soil CO_2 concentration along the Las Maquinas (LM) profile. SP maximum and CO_2 and T peaks are numbered XIX, and represent the hydrothermal system. The dotted lines represent the main and secondary faults.

2002). Therefore, rock alteration could explain the SP minima in Cabañita.

In the hydrogeological zones referred to as HG1 through HG4, both F8 and CF3 faults delimit two plateaus (Fig. 5). As for the Las Maquinitas-Las Maquinas profile (Fig. 4), F8 is thought to separate two aquifers located at two different depths (defined by the low SP variation from 70–80 mV to 100–120 mV). The second plateau observed (from 10 mV to 70–80 mV), delimited by CF3, shows a gradual decrease in SP that could be related to the increase in thickness of the vadose zone (Aubert and Atangana, 1996; Bennati et al., 2011) due to the increasing elevation in this sector of the profile. In areas HG1 and HG4, the main faults, LMMF1 and CF2, oriented NE, are indicated in previous profiles as preferential pathways for fluid ascent, and show a small CO_2 peak and SP minima. This means that, in the SE portion of Cabañita, these main faults may no longer be the main structures controlling the heat and fluid transfer to the surface (Finizola et al., 2002). This may imply that these faults are less deeply rooted or that the hydrothermal reservoir is deeper. However, the small CO_2 maxima observed to correspond with the CF2 fault suggests that it is still a permeable pathway, driving the hydrothermal gases up to the surface. Furthermore, the continuity of the main fault, CF1 (from AF-COP-LMM profile), shows small SP and CO_2 maxima, indicating that the end of the CF1 fault is still able to provide a small part of the heat energy measured at the surface. Finally, a succession of SP minima observed along the Las Maquinitas-Las Maquinas profile (Fig. 4) is also observed in the present profile (F13, F6, F7, F8, F9, F10, F14, F15, F16; Fig. 4), coinciding with NE-striking small fractures or secondary faults, as observed in the satellite image.

4.3.4. Profile AF

The Anfiteatro (AF) profile (Fig. 6) is located inside the extensional structure (blue profile in Fig. 2), where geothermal activity and associated alteration zones are observed.

Three hydrothermal zones (XVI, XVII and XVIII) are defined by CO_2 peaks (up to 3000 ppm), but are not necessary associated with T-SP peaks. This reflects the low input of fluids from depth and argues for a decreasing heat energy at depth (Finizola et al., 2002). The absence of SP-T and CO_2 signals at the beginning of this profile is followed by a slight increase in SP-CO_2-T maxima at 60–70 m (e.g., XVI; grey field; Fig. 6). This suggests the absence of underground fluid flow, possibly due to the presence of altered rocks observed in the field that act as natural impermeable barriers to fluids (Barde-Cabusson et al., 2009; Finizola et al., 2003; Revil et al., 2002). A SP maximum with the absence of CO_2 and T anomalies, referred to as OS1 (also observed in the AF-COP-LMM profile; Fig. 3), is interpreted as an old structural limit, producing a reversed SP peak due to downward fluid flow through alteration minerals (Guichet et al., 2006). Finally, the presence of the AFF2 fault (oriented NW) is characterized by an abrupt decrease in both CO_2 and SP.

4.3.5. Profile LM

The Las Maquinas (LM; Fig. 7) profile shows two main features, also observed in the LM-CB-AF profile (Fig. 5). First, the SP, CO_2, and T maxima observed at 60 m and 80 m, illustrate the lithological transition from the ignimbrite to the upper lava unit of the Las Mellizas sequence. The absence of CO_2 and T peaks SW of L1 indicates that the upper lava unit is completely impermeable to fluid ascent, as observed in the LM-CB-AF profile. This is also supported by the presence of positive SP

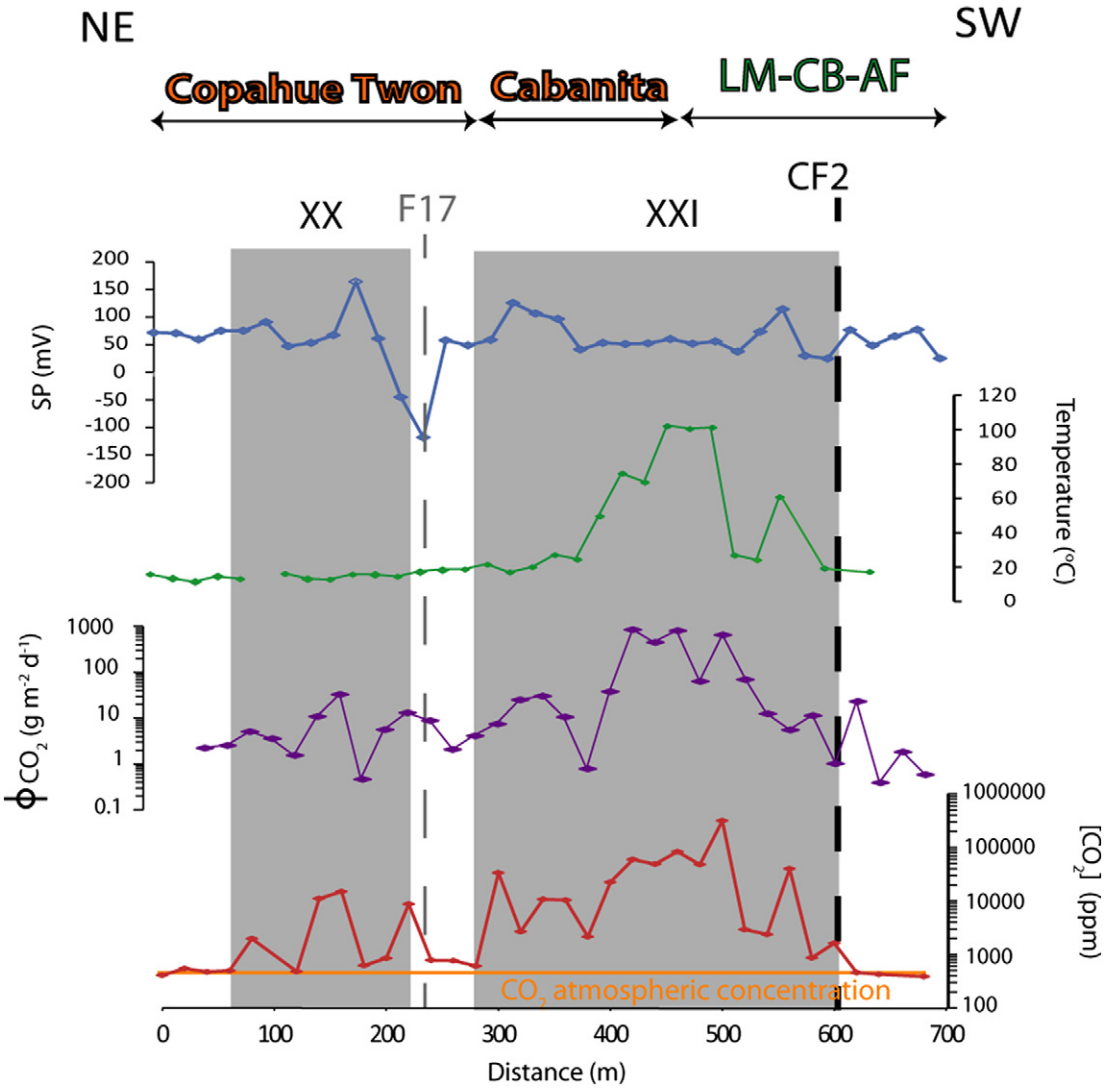

Fig. 8. Self-potential (SP), soil temperature, soil CO_2 flux, and soil CO_2 concentration along the Copahue Town – Cabañita (COP-CB) profile. SP maximum and CO_2 and T peaks are numbered XX, XXI and represent the hydrothermal system. L1 represents the lithological variation observed between upper lava and ignimbrites from the Las Mellizas sequence. The dotted lines represent the main and secondary faults.

peaks in this area (Fig. 5), and the presence of visible rock alteration at the surface. The second break in the SP signal (at 240 m) might show the presence of fault F11, revealed in our study to be oriented WNW (Fig. 7). Additionally, taking the CO_2 data into account, this fault does not seem to be involved in fluid ascent.

4.3.6. Profile COP-CB

The Copahue Town-Cabañita (COP-CB) profile is presented in Fig. 8. As was observed in the LM-CB-AF profile, the limit of the Cabañita geothermal area is highlighted by a CO_2 maximum, which highlights the presence of the main fault, CF2 (Melnick et al., 2006), and the secondary F17 fault, both NE-oriented. The Cabañita area is characterized by positive CO_2 and T peaks, representing large volumes of rising hydrothermal fluids. However, the decreasing of SP associated with the CO_2 and T maxima at the center of this area probably suggests an impermeable layer, likely composed of altered rocks. Small positive SP and CO_2 peaks are observed in the geothermal area referred to as XX in Fig. 8. This area is located between the main geothermal zones of Copahue Town and Cabañita, and appears to represent a transition zone, where geothermal activity is lower.

5. Discussion

For the first time, a complete SP map, coupled with soil CO_2 fluxes and concentrations, $^3He/^4He$ ratios, and T data of a CCVC geothermal area located NE of Copahue volcano is available. A brief summary of the main features follows. The geothermal area of North-East Copahue volcano can be divided in three groups according to SP-CO_2-T and He features: 1) Las Maquinas, Las Maquinitas, Cabañita and Copahue Town present particularly high CO_2 concentration values (up to 591,969 ppm; Figs. 3 to 5). In these four zones, high temperatures and Rc/Ra (93 °C and up to 8.16 ± 0.21 Ra respectively) correspond with low positive SP anomalies; 2) Anfiteatro, which is delimited by two compressive WNW-striking faults, shows low CO_2 concentrations (up to 58,292 ppm; Figs. 3 and 6) and moderate temperature and Rc/Ra values (51 °C, 4.63 ± 0.10 Ra and 5.12 ± 0.05 Ra respectively), which are consistent with the observed low fumarolic and bubbling gas emanations, referred to as AF4 and AF2. The 2016 sampling campaign in this sector revealed particularly high Rc/Ra values (7.17 ± 0.20 Ra at AF3) never before observed at the eastern edge of Anfiteatro, and correlated with a moderate peak in CO_2 concentration (50,982 ppm to 58,292 ppm); 3) in the hydrogeological areas (Figs. 3 to 5), CO_2

concentrations are usually atmospheric (~400 ppm), and temperatures are close to the ambient temperature at the time of the field campaign (~17 °C). Furthermore, the SP signal is explained by a water infiltration along small fractures and by the water-table elevation in areas HG1–HG2 (Figs. 4 and 5) and HG3–HG6 (Figs. 3 to 5).

In the following sub-sections, the complete dataset will be used to characterize the fracture/fault controls on the evolution of the active geothermal system, and to define the deep fluid versus meteoric water circulation patterns.

5.1. Fluid circulation in the CCVC geothermal system: implication of a vapor-dominated zone and the geothermal reservoir

The first studies of the chemistry of the CCVC were carried out from a geothermal exploration perspective (Jurío, 1977; Panarello et al., 1988; Pesce, 1989; Sierra et al., 1992), followed closely by a magneto-telluric survey (JICA, 1992). The CCVC geothermal field is defined as a vapor-dominated field, with stratified layers connected by fractures with increased vertical permeability. During geothermal exploration at the CCVC, a vapor-dominated hydrothermal system was recognized in the northeastern area. It is composed of two different productive reservoirs, located at depths of 800–1000 m (vapor-dominated zone) and 1400 m (hydrothermal reservoir), with estimated temperatures of 200 °C and 250 °C–300 °C respectively (Agusto et al., 2013; Panarello et al., 1988; Panarello, 2002). As proposed by Agusto et al. (2013) and Roulleau et al. (2015a, 2016), the main fumarolic emissions observed in the CCVC originate from the boiling of a geothermal reservoir fed mainly by meteoric water recharge. Recently, Chiodini et al. (2015) proposed a unique vapor-dominated zone feeding the CCVC geothermal manifestations, located between Copahue, Las Maquinas, and the tentatively exploited area where COP-1, COP-2, and COP-3 geothermal wells are located.

Fig. 9 shows the map of soil CO_2 concentrations and Rc/Ra ratios for the study area. As was observed in the SP, CO_2, and T profiles (Figs. 3 to 8), high CO_2 concentrations (up to 380,000 ppm for Las Maquinitas) and high diffusive CO_2 flux (1709 $g \cdot m^{-2} \cdot d^{-1}$; Figs. 3 to 5) are located in the main geothermal areas, such as Cabañita, Copahue Town, Las Maquinitas, and Las Maquinas, where Rc/Ra is high (up to 8.16 Ra), practically identical to a pure MORB-type mantle source (8 ± 1 Ra). These high values may also be observed in some subduction zones (Hilton et al., 2002), such as in Japan (Roulleau et al., 2013; Roulleau et al., 2015b), although they usually tend to show lower values by assimilation of radiogenic helium from the subducting plate (Sano et al., 2006). Anfiteatro shows lower CO_2 concentrations (up to 58,292 ppm) and moderate Rc/Ra (up to 5.12 Ra), suggesting a limited ascent of hydrothermal fluids. However, the new gas sample collected in 2016 at the eastern limit of Anfiteatro presents a high Rc/Ra (7.17 ± 0.20 Ra), comparable to the other geothermal areas of the Copahue geothermal system. Fig. 10 presents a conceptual model of the CCVC geothermal system, where the different layers are represented (i.e., the argillic zone, the vapor-dominated zone, and the hydrothermal reservoir; JICA, 1992). The main geothermal area (Cabañita, Copahue, Las Maquinitas, and Las Maquinas; referred to as the "Fumarole zone" in Fig. 9) is characterized by a shallower depth of the vapor-dominated zone, 1900–1700 m a.s.l., and is associated with high Rc/Ra (7.10 Ra–8.16 Ra). The deep wells, COP-1 and COP-2, appear to pump fluids from a deeper vapor-dominated zone, at approximately 1300–1200 m, and show high Rc/Ra (7.51 ± 0.06 Ra), similar to the values measured in the "Fumarole zone". In fact, these deep wells provide direct information on the hydrothermal system. They have an average depth of ~1500 m, reaching the deeper reservoir with higher temperatures (250–300 °C; Agusto et al., 2013; Panarello, 2002), as well as the shallow vapor-dominated zone (200 °C; Sierra et al., 1992; Panarello, 2002). However, in this area, no recent hydrothermal activity is observed, suggesting that the hydrothermal fluids cannot pass through the impervious argillic rocks observed at 500 m depth.

On the other hand, Anfiteatro might be located in a transitional zone; the eastern part of Anfiteatro seems to be at the limit of the high vapor zone (Fig. 9), whereas in the central and western sectors of Anfiteatro, the vapor-dominated zone is deeper (elevation ~1500 m a.s.l.; Figs. 7–8; JICA, 1992). The low CO_2 concentration (58,292 ppm), lower T (51 °C), and moderate Rc/Ra (4.64 ± 0.10 Ra to 5.13 ± 0.05 Ra.) suggest the presence of a thicker clayey alteration zone, impermeable to fluid flow. The AF-COP-LMM profile shows the presence of a cold aquifer close to the surface, to the east of Anfiteatro (Fig. 3), and water accumulation at the surface inside Anfiteatro, suggesting that meteoric water is predominant. The interaction between water, bedrock and deep fluids

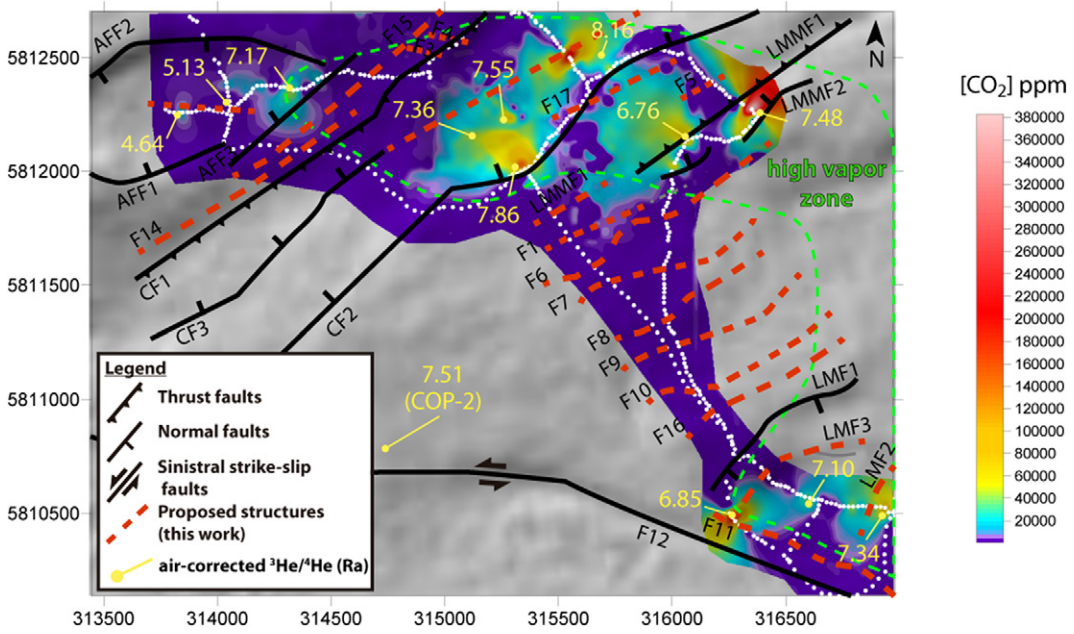

Fig. 9. Map of the soil CO_2 concentrations for the CCVC geothermal system (map coordinates in m, UTM-WGS84 19S). The air-corrected $^3He/^4He$ ratios (Rc/Ra) are added for each geothermal area, and part are from Roulleau et al. (2016). The elevated vapor zone (elevation ~1900–1700 m) is defined using the geophysical study from JICA (1992). White dots represent the locations of CO_2 measurements. Local structural limits are added from previous works (known faults; Rojas Vera et al., 2009; Melnick et al., 2006) and from this study (new faults), with their names.

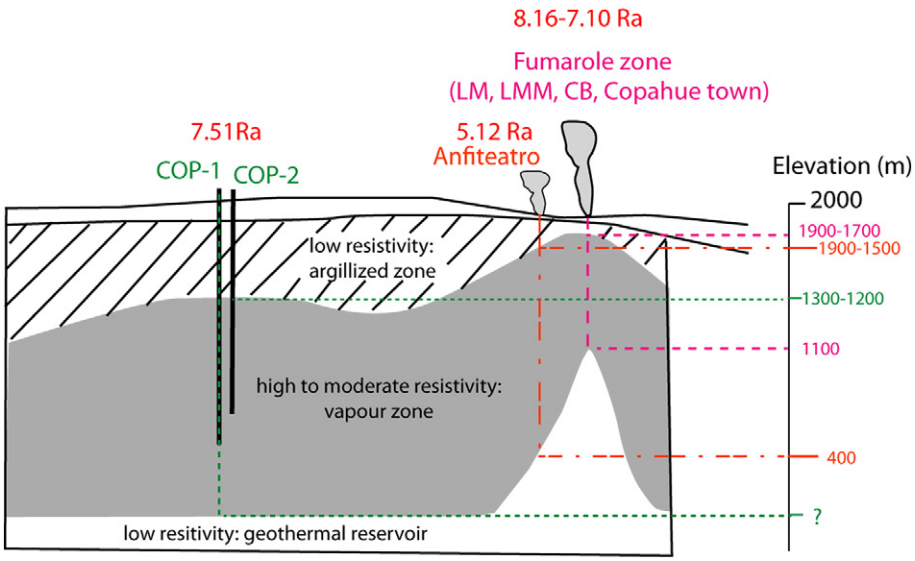

Fig. 10. Conceptual model of the CCVC geothermal system. The air-corrected $^3He/^4He$ ratios (Rc/Ra) are added. "Fumarole zone" represents the main active geothermal area, including Cabañita, Copahue, Las Maquinitas, and Las Maquinas. Resistivity model from JICA (1992).

may produce the decrease in CO_2 concentrations (and fluxes), temperature, and Rc/Ra, as observed in Anfiteatro. A unique vapor-dominated zone feeding the geothermal manifestations is also supported by the current results, as proposed by Chiodini et al. (2015), but possibly extending until Anfiteatro. However, this unique vapor-dominated zone seems efficient regarding hydrothermal fluid flow only when it is shallower (elevation of 1900–1700 m).

5.2. Relationship between SP, CO_2, T, $^3He/^4He$, and faults: implications for fluid circulation

By combining the SP, soil CO_2, temperatures, and helium isotopes, a conceptual model summarizing the fluid circulation pattern of the investigated area is proposed.

The CCVC is located where the LOFS bends eastward and decomposes into a series of NNW- to NE-striking extensional and trans-tensional faults with a horsetail-like geometry (Rosenau et al., 2006). The associated damage zone, as asserted by some authors (Rowland and Simmons, 2012; Tardani et al., 2016), promotes high permeability and vertical fluid circulation, facilitating the appearance of superficial geothermal manifestations. It therefore plays a key role as a host structure, focusing increased fluid flow in geothermal systems. The magneto-telluric survey of the CCVC geothermal system (JICA, 1992) suggests that the NE-striking faults are a group of recent faults associated with the volcanic activity of Copahue volcano (Mid-Pleistocene), and are considered to act as pathways for hydrothermal fluids in Copahue, Anfiteatro, Las Maquinitas, and Cabañita. The WNW-striking faults seem to be extensional in Paso de Copahue and Lago Agrio, and therefore act as pathways for the hydrothermal fluids of Las Maquinas and Chancho-có.

Fig. 9 presents the complete fault network of the CCVC, and comprises a compilation of mapped and inferred faults and structures deduced from the SP, CO_2, and T measurements of this study, superposed on the soil CO_2 concentration map. The main geothermal areas reporting high CO_2 degassing and Rc/Ra, Cabañita, Copahue, Las Maquinitas, and Las Maquinas, are located where the main NE-striking faults are observed (Melnick et al., 2006; Rojas Vera et al., 2009), suggesting that they are located along these structural discontinuities (e.g., CF2, CF1, LMMF1, LMMF2, LMF1, LMF2 and LMF3). This is consistent with the fact that the hydrothermal fluids in the north of the SVZ represent the most primitive magmatic signatures (Agusto et al., 2013; Hilton et al., 1993; Ray et al., 2009; Roulleau et al., 2015a; Roulleau et al., 2016; Tardani et al., 2016), likely transmitted to the shallow volcanic/geothermal area along the NNE-striking LOFS (Rosenau et al., 2006; Sanchez et al., 2013; Tardani et al., 2016). Anfiteatro is a pull-apart basin, delimited to the east by a small NE-striking fault, called AFF3 (SP-CO_2 maxima and high Rc/Ra), and located at the NW limit of the high vapor zone (Fig. 9). Weak geothermal activity along this fault, AFF3, was demonstrated in the current work. The NE-striking faults therefore represent a preferential pathway for hydrothermal fluid flow. The end of these faults (e.g., CF1, CBF1, LMMF1), west of Copahue, shows small SP and CO_2 concentration positive anomalies, but without visible hydrothermal manifestations at the surface (Figs. 4, 5). This could be explained by the fact that either 1) the high vapor zone limit (Fig. 9) is located north of these faults, and the heat energy is at a lower depth, and/or 2) the permeability of these faults is variable, and could be lower west of the Copahue volcano. The small NE-striking faults and/or fractures (F10, F9, F8, F7, F6, F13, and F5), observed in Figs. 3, 4, and 5 in the main profiles (SE of Copahue), seem to be inefficient regarding the ascent of hydrothermal fluids, likely because they are shallower and guide only meteoric water downward to the aquifer.

WNW-striking faults are observed in Anfiteatro (AFF1, AFF2, OS1; Fig. 3) and SW of Las Maquinas (F11, F12; Fig. 5). In Anfiteatro, AFF1 and AFF2 faults show small SP maxima, whether or not associated with CO_2 maxima (Figs. 3 and 6), suggesting little ascent of hydrothermal fluids. OS1 presents as an old fault, oriented WNW (SP maximum, with no T or CO_2 anomalies), and currently altered in argillic facies. The observed positive SP peak corresponds to the reverse negative polarity due to water infiltration through calcite (Brothelande et al., 2014; Guichet et al., 2006), while hydrothermal fluids are not rising in this area anymore. In Las Maquinas, the WNW-trending faults (F11 and F12; Fig. 5) located to the SE of this area, are highlighted by CO_2, T, and SP minima, and are likely evidence of water infiltration. For Anfiteatro and the western part of Las Maquinas, the vapor-dominated zone is deeper (altitude ~1600–1500 m; Figs. 9 and 10), supporting the hypothesis that these faults are not effective at guiding the hydrothermal fluids to the surface. As proposed by Tardani et al. (2016) and Sanchez et al. (2013) at the regional scale, the WNW-striking faults seem to promote the formation of long-lived, more evolved high-enthalpy geothermal systems due to increased residence times of the hydrothermal fluids at depth. This could explain the moderate Rc/Ra observed in Anfiteatro. The WNW-striking faults would therefore inhibit high vertical fluid flow and promote a shallow mixing between the hydrothermal fluids and meteoric water. These structures appear to be the southern limit discontinuities of the Copahue geothermal system.

6. Conclusions

In this work, fluid circulation of the geothermal area within the CCVC was studied by using a dense coverage of SP, and soil CO_2 and temperature data. The observed patterns of SP, CO_2, and T anomalies, and $^3He/^4He$ ratios reflect the combined effects of local and regional tectonic structures, which exert a strong control on fluid circulation. The model proposed involves: 1) the ascent of hydrothermal fluids along the NE-striking faults, dependent on the lower depth of the vapor-dominated zone (1900–1700 m a.s.l.); and 2) freshwater infiltration and interaction along WNW-trending faults in the geothermal area (Anfiteatro and west of Las Maquinas) and along secondary NE-trending faults in the hydrogeological area, where the vapor-dominated zone is deeper (~1500 m). A unique and highly vapor-dominated zone is therefore defined through the main geothermal area, but with limited extension to the east of Anfiteatro, where a high helium ratio is observed. The high $^3He/^4He$ ratios (up to 8.13 Ra) suggest a deep magmatic origin, while, in Anfiteatro, moderate $^3He/^4He$ ratio (up to 5.10 Ra) support a transitional zone illustrating the low ascent of the hydrothermal fluids. The NE-striking faults, associated with the volcano tectonic activity of Copahue volcano, represent a preferential pathway for hydrothermal fluid flow and CO_2 degassing. In contrast, the WNW-striking faults seem to be the preferential structures for meteoric water-hydrothermal fluid interaction at shallow depth, and seem to limit the Copahue geothermal area to the south.

Acknowledgments

We wish to thank Eric Delcher for his help during the construction of the CO_2 equipment and Vicente Solar for supplying the diffusive CO_2 flux equipment. Thanks to Dr. Finizola for his help with the dataset. E. Roulleau was funded through FONDECYT project 11130351 and a ClerVolc-Auvergne Fellowship. This work was partially funded by CEGA (led by *D. morata*) via FONDAP project 15090013. M. Pizarro was funded by a PhD grant from CONICYT-PCHA/doctorado Nacional/2014-21240597. D. Tardani's contribution was funded by FONDECYT project 1130030 (M. Reich). D. L. Pinti was funded by NSERC Discovery Grant no. 1173913. Part of the data in this paper constituted the Bachelor's thesis of F. Bravo.

References

Agusto, M., 2011. Estudio geoquímico de los fluidos volcánicos e hidrotermales del Complejo Volcánico Copahue Caviahue y su aplicación para tareas de seguimiento 270 pp. (Ph.D. Thesis).

Agusto, M., et al., 2007. Chemical and isotopic features of thermal fluid discharges in the volcano-hydrothermal system of Caviahue-Copahue volcanic complex (Argentina). GEOSUR (International Geological Congress on the Southern Hemisphere) edited, Santiago de Chile.

Agusto, M., Tassi, F., Caselli, A.T., Vaselli, O., Rouwet, D., Capaccioni, B., Caliro, S., Chiodini, G., Darrah, T., 2013. Gas geochemistry of the magmatic-hydrothermal fluid reservoir in the Copahue-Caviahue Volcanic Complex (Argentina). J. Volc. Geotherm. Res. 257 (0), 44–56.

Alam, M.A., Sánchez, P., Parada, M.A., 2010. Interplay of volcanism and structural control in defining the geothermal system(s) along the Liquiñe-Ofqui Fault Zone, in the south-central Chile. Geoth. Res. Counc. (GRC) Trans. 34, 747–750.

Aravena, D., Muñoz, M., Morata, D., Lahsen, A., Parada, M.A., Dobson, P., 2016. Assessment of high enthalpy geothermal resources and promising areas of Chile. Geothermics 59: 1–13. http://dx.doi.org/10.1016/j.geothermics.2015.09.001.

Arnórsson, S., 1995. Geothermal systems in Iceland: structure and conceptual models. High temperature areas. Geoth 24, 561–602.

Arnórsson, S., Stefansson, A., Bjarnason, J.O., 2007. Fluid-fluid interactions in geothermal systems. Rev. Mineral. Geochem. 65, 259–312.

Aubert, M., 1999. Practical evaluation of steady heat discharge from dormant active volcanoes: case study of Vulcarolo fissure (Mount Etna, Italy). J. Volc. Geotherm. Res. 92, 413–429.

Aubert, M., Atangana, Q.Y., 1996. Self-potential method in hydrogeological exploration of volcanic areas. Ground Water 34 (6), 1010–1016.

Barde-Cabusson, S., Finizola, A., Revil, A., Ricci, T., Piscitelli, S., Rizzo, E., Angeletti, B., Balasco, M., Bennati, L., Byrdina, S., Carzaniga, N., Crespy, A., Di Gangi, F., Morin, J., Perrone, A., Rossi, M., Roulleau, E., Suski, B., Villeneuve, N., 2009. New geological insights and structural control on fluid circulation in La Fossa cone (Vulcano, Aeolian Islands, Italy). J. Volc. Geotherm. Res. 185 (3), 231–245.

Bennati, L., Finizola, A., Walker, J.A., Lopez, D.L., Higuera-Diaz, I.C., Schütze, C., Barahona, F., Cartagena, R., Conde, V., Funes, R., Rios, C., 2011. Fluid circulation in a complex volcano-tectonic setting, inferred from self-potential and soil CO_2 flux surveys: the Santa Maria-Cerro Quemado-Zunil volcanoes and Xela caldera (northwestern Guatemala). J. Volc. Geotherm. Res. 199 (3–4), 216–229.

Birkle, P., Marín, E.P., Pinti, D.L., Castro, M.C., 2016. Origin and evolution of geothermal fluids from Las Tres Vírgenes and Cerro Prieto fields, Mexico — co-genetic volcanic activity and paleoclimatic constraints. Appl. Geochem. 65, 36–53.

Bolós, X., Barde-Cabusson, S., Pedrazzi, D., Martí, J., Casas, A., Lovera, R., Nadal, D., 2014. Sub-surface geology in the monogenetic La Garrotxa Volcanic Field (NE Iberian Peninsula). Int. J. Earth Sci. http://dx.doi.org/10.1007/s00531-014-1044-3 (online in June 2014).

Brothelande, E., Finizola, A., Peltier, A., Delcher, E., Komorowski, J.C., Di Gangi, F., Borgogno, G., Passarella, M., Trovato, C., Legendre, Y., 2014. Fluid circulation pattern inside La Soufriere volcano (Guadeloupe) inferred from combined electrical resistivity tomography, self-potential, soil temperature and diffuse degassing measurements. J. Volc. Geotherm. Res. 288, 105–122.

Caselli, A.T., Agusto, M.R., Fazio, A., 2005. Cambios térmicos y geoquímicos del lago cratérico del volcán Copahue (Neuquén): posibles variaciones cíclicas del sistema volcánico. Actas del Congreso XVI Congreso Geológico Argentino 1, pp. 332–336 (La Plata).

Cembrano, J., Lara, L., 2009. The link between volcanism and tectonics in the southern volcanic zone of the Chilean Andes: a review. Tectonics 471, 96–113.

Cembrano, J., Beck, M.E., Burmester, R.F., Rojas, C., Garcia, A., Herve, F., 1992. Paleomagnetism of lower cretaceous rocks from east of the Liquiñe-Ofqui fault zone, southern Chile: evidence of small in-situ clockwise rotations. Earth Planet. Sci. Lett. 113, 539–551.

Cembrano, J., Herve, F., Lavenu, A., 1996. The Liquiñe-Ofqui fault zone: a long-lived intra-arc fault system in southern Chile. Tectonics 259, 55–66.

Cembrano, J., Shermer, E., Lavenu, A., Sanueza, A., 2000. Contrasting nature of deformation along an intra-arc shear zone, the Liquiñe-Ofqui fault system, southern Chilean Andes. Tectonics 319, 129–149.

Chiodini, G., Cioni, R., Guidi, M., Raco, B., Marini, L., 1998. Soil CO_2 flux measurements in volcanic and geothermal areas. Appl. Geochem. 13, 543–552.

Chiodini, G., Cardellini, C., Lamberti, M.C., Agusto, M., Caselli, A., Liccioli, C., Tamburello, G., Tassi, F., Vaselli, O., Caliro, S., 2015. Carbon dioxide diffuse emission and thermal energy release from hydrothermal systems at Copahue-Caviahue Volcanic Complex (Argentina). J. Volc. Geotherm. Res. 304, 294–303.

Corwin, R.F., Hoover, D.B., 1979. The self-potential method in geothermal exploration. Geophysics 44, 226–245.

Cox, S., 2010. The application of failure mode diagrams for exploring the roles of fluid pressure and stress states in controlling styles of fracture-controlled permeability enhancement in faults and shear zones. Geofluids 10, 217–233.

Craig, H., Lupton, J.E., Horibe, Y., 1978. A mantle helium component in Circum-Pacific volcanic gases: Hakone, the Marianas, and Mr. Lassen. In: E. C. Advances in Earth and Planetary Science; Alexander, Ozima, M. (Ed.), Terrestrial rare Gases. Academic publication, Japan, pp. 3–16.

Di Maio, R., Berrino, G., 2016. Joint analysis of electric and gravimetric data for volcano monitoring. Application to data acquired at Vulcano Island (southern Italy) from 1993 to 1996. J. Volcanol. Geotherm. Res. 327 (15), 459–468.

Finizola, A., Sortino, F., Lenat, J.F., Valenza, M., 2002. Fluid circulation at Stromboli volcano (Aeolian Islands, Italy) from self-potential and soil gas surveys. J. Vol. Geotherm. Res. 116 (1–2), 1–18.

Finizola, A., Sortino, F., Lenat, J.F., Aubert, M., Ripepe, M., Valenza, M., 2003. The summit hydrothermal system of Stromboli. New insights from self-potential, temperature, CO_2 and fumarolic fluid measurements, with structural and monitoring implications. BVol 65 (7), 486–504.

Finizola, A., Lenat, J.F., Macedo, O., Ramos, D., Thouret, J.C., Sortina, F., 2004. Fluid circulation and structural discontinuities inside Misti volcano (Peru) inferred from self-potential measurements. J. Volcanol. Geotherm. Res. 135 (4), 343–360.

Goff, F., Janik, C.J., 2000. Geothermal systems. In: Sigurdsson, H., Houghton, B., McNutt, S., Rymer, H., Stix, J. (Eds.), Encyclopedia of Volcanoes. Academic Press, San Diego, CA, pp. 817–834.

Guichet, X., Journiaux, L., Catel, N., 2006. Modification of streaming potential by precipitation of calcite in a sand-water system: laboratory measurements in the pH range from 4 to 12. GeoJI 166 (1), 445–460.

Harris, A.J.L., Maciejewski, A.J.H., 2000. Thermal surveys of the Vulcano Fossa fumarole field 1994 – 1999: Evidence for fumarole migra-tion and sealing. J. Volcanol. Geotherm. Res. 102, 119–147.

Hauser, A., 1997. Catastro y Caracterización de las Fuentes de Aguas Minerales y Termales de Chile, SERNAGEOMIN, Boletín N°50 (99pp).

Hilton, D.R., Hammerschmidt, K., Teufel, S., Friedrichsen, H., 1993. Helium isotope characteristics of Andean geothermal fluids and lavas. Earth Planet. Sci. Lett. 120 (3–4), 265–282.

Hilton, D.R., Fischer, T.P., Marty, B., 2002. Noble gases and volatile recycling at subduction zones. In: D. P. Reviews in Mineralogy and Geochemistry; Porcelli, Ballentine, C.J, and Wieler, R. (Ed.), Noble gases in Geochemistry and Cosmochemistry, pp. 319–370.

JICA, 1992. The Feasibility Study on the Northern Neuquen Geothermal Development Project. Japan International Cooperation Agency, Neuquen, p. 444.

Jurío, R.L., 1977. Características geoquímicas de los fluidos termales de Copahue (Neuquén - Argentina). Principales implicancias geotérmicas, Apartado de la revista "Minería". p. 172.

Kerrick, D.M., McKibben, M.A., Seward, T.M., Caldeira, K., 1995. Convective hydrothermal CO_2 emission from high heat flow regions. Chem. Geol. 121, 285–293.

Kiryukhin, A.V., 2013. A modeling study of the role of hydrothermal processes in the formation of production reservoirs in volcanogenic rocks. Procedia Earth Planet. Sci. 7, 436–439.

Lahsen, A., 1988. Chilean geothermal resources and their possible utilization. Geothermics 17, 401–410.
Linares, E., Ostera, H.A., Mas, L., 1999. Cronología Potasio-Argón del complejo efusivo Copahue-Caviahue, Provincia de Neuquén. Rev. Asoc. Geol. Argent. 54 (3), 240–247.
Matsushima, N., Michiwaki, M., Okazaki, N., Ichikawa, R., Takagi, A., Nishida, Y., Mori, H.Y., 1990. Self-Potential Studies in Volcanic Areas(2): Usu, Hokkaido Komaga-take and Me-akan. J. Fac. Sci., Hokkaido Univ. Ser. 7, Geophys. 8 (5), 465–477.
Melnick, D., Folguera, A., Ramos, V.A., 2006. Structural control on arc volcanism: the Caviahue-Copahue complex, central to Patagonian Andes transition (38°S). JSAES 22 (1–2), 66–88.
Muñoz, J., Stern, C., 1988. The quaternary volcanic belt of the sourthern continental margin of South America: transverse structural and petrochemical variations across the segment between 38° and 39°S. JSAES 1, 147–161.
Nakanishi, S., Abe, M., Todaka, N., Yamada, M., Sierra, J.L., Gingins, M.O., Mas, L.C., Pedro, G.E., 1995. Copahue geothermal system, Argentina — study of a vapor-dominated reservoir. Proceedings of the World Geothermal Congress 95. Vol. 2, pp. 1167–1172.
Onizawa, S., Matsushima, N., Ishido, T., Hase, H., Takakura, S., Nishi, Y., 2009. Self-potential distribution on active volcano controlled by three-dimensional resistivity structure in Izu-Oshima, Japan. Geophys. J. Int. 178 (2), 1164–1181.
Panarello, H.O., 2002. Características isotópicas y termodinámicas de reservorio del campo geotérmico Copahue-Caviahue, provincia del Neuquén. Rev. Asoc. Geol. Argent. 57 (2), 182–194.
Panarello, H.O., Levin, M., Albero, M.C., Sierra, J.L., Gingins, M.O., 1988. Isotopic and geochemical study of the vapour dominated geothermal field of Copahue (Neuquén, Argentina). Revista Brasileira de Geofisica 5 (2), 275–282.
Parada, M.A., López-Escobar, L., Oliveros, V., Fuentes, F., Morata, D., et al., 2007. Andean magmatism. In: Gibson, T.M.A.W. (Ed.), The Geology of Chile. The Geological Society of London, pp. 115–146.
Pesce, A., 1989. Evolución volcano-tectónica del complejo efusivo Copahue-Caviahue y su modelo geotérmico preliminar, Asociación Geológica Argentina. Theol. Rev. 44 (1–4), 307–327.
Ray, M.C., Hilton, D.R., Munoz, J., Fischer, T.P., Shaw, A.M., 2009. The effects of volatile recycling, degassing and crustal contamination on the helium and carbon geochemistry of hydrothermal fluids from the Southern Volcanic Zone of Chile. Chem. Geol. 266 (1–2), 38–49.
Revil, A., Hermite, D., Spangenberg, E., Cochemé, J.J., 2002. Electrical properties of Zeolitized volcaniclastic material. J. Geo. Res. 107 (B8), 2168.
Revil, A., Finizola, A., Piscitelli, A., Rizzo, E., Ricci, T., Crespy, A., Angeletti, B., Balasco, M., Barde Cabusson, S., Bennati, L., Bolève, A., Byrdina, S., Carzaniga, N., Di Gangi, F., Morin, J., Perrone, A., Rossi, M., Roulleau, E., Suski, B., 2008. Inner structure of La Fossa di Vulcano (Vulcano Island, southern Tyrrhenian Sea, Italy) revealed by high resolution electric resistivity tomography coupled with self-potential, temperature, and soil CO_2 diffuse degassing measurements. J. Geophys. Res. 113. http://dx.doi.org/10.1029/2007JB005394.
Roche, O., Druit, T., Merle, O., 2000. Experimental study of caldera formation. J. Geophys. Res.: Solid Earth 105 (B1), 395–416.
Rojas Vera, E., Folguera, A., Spagnuolo, M., Gimenez, M., Ruiz, F., Martinez, P., Ramos, V.A., 2009. La neotectonica del arco volcanico a la latitud del volcan Copahue (38°S). Andes de Neuquen, Revista de la Asociacion Geologica Argentina 65, 204–214.
Rosenau, M., Melnick, D., Echtler, M., 2006. Kinematic constraints on intra-arc shear and strain partitioning in the southern Andes between 38°S and 42°S latitude. Tectonics 25 (TC4013).
Roulleau, E., Sano, Y., Takahata, N., Kawagucci, S., Takahashi, H., 2013. He, N and C isotopes and fluxes in Aira caldera: comparative study of hydrothermal activity in Sakurajima volcano and Wakamiko crater, Kyushu, Japan. J. Volc. Geotherm. Res. 258, 163–175.
Roulleau, E., Tardani, D., Vinet, N., Sano, Y., Takahata, N., Reich, M., 2015a. Noble-Gas and Nitrogen Isotope Geochemistry of Geothermal Fluids from the Caviahue-Copahue Volcanic Complex in the Southern Andes (Paper Presented at Goldschmidt Prague (CZ), 08/2015).
Roulleau, E., Vinet, N., Sano, Y., Takahata, N., Shinihara, H., Ooki, M., Takahashi, H.A., Furukawa, R., 2015b. Effect of the volcanic front migration on helium, nitrogen, argon, and carbon geochemistry of hydrothermal/magmatic fluids from Hokkaido volcanoes, Japan. Chem. Geol. 414, 42–58.
Roulleau, E., Tardani, D., Sano, Y., Takahata, N., Vinet, N., Bravo, F., Munoz, C., Sanchez, J., 2016. New insight from noble gas and stable isotopes of geothermal/hydrothermal fluids at Caviahue-Copahue Volcanic Complex: boiling steam separation and water-rock interaction at shallow depth. J. Volc. Geotherm. Res. 328, 70–83.
Rowland, J.V., Simmons, S.F., 2012. Hydrologic, magmatic, and tectonic controls on hydrothermal flow, Taupo Volcanic Zone, New Zealand: implications for the formation of epithermal vein deposits. Econ. Geol. 107, 427–457.
Sanchez, P., Perez-Flores, P., Arancibia, G., Cembrano, J., Reich, M., 2013. Crustal deformation effects on the chemical evolution of geothermal systems: the intra-arc Liquiñe-Ofqui fault system, southern Andes. Int. Geol. Rev. 55 (11).
Sano, Y., Wakita, H., 1988. Helium isotope ratio and heat discharge rate in the Hokkaido Island, Northeast Japan. Geochem. J. 22, 293–303.
Sano, Y., Takahata, N., Seno, T., 2006. Geographical distribution of $^3He/^4He$ ratios in the Chugoku District, Southwestern Japan. PApGe 163, 745–757.
Sano, Y., Tokutake, T., Takahata, N., 2008. Accurate measurement of atmospheric helium isotopes. Anal. Sci. 24 (4), 521–525.
Sano, Y., Marty, B., Burnard, P., 2013. Noble gas in the Atmosphere. In: Burnard, P. (Ed.), The Noble Gases as Geochemical Tracers.
Sasai, Y., Zlotnicki, J., Nishida, Y., Yvetot, P., Murakami, H., Tanaka, Y., Ishikawa, Y., Koyama, S., Sekiguchi, W., 1997. Electromagnetic monitoring of Miyake-jima Volcano, Izu-Bonin Arc, Japan: a preliminary report. J. Geomagn. Geoelectr. 49, 1293–1316.
Sepúlveda, F., Lahesen, A., Bonvalot, S., Cembrano, J., Alvarado, A., Letelier, P., 2005. Morphostructural evolution of the Cordon Caulle geothermal region, Southern Volcanic Zone, Chile: insights from gravity and Ar-40/Ar-39 dating. J. Volc. Geotherm. Res. 148, 165–189.
Sibson, R.H., 1996. Structural Permeability of Fluid-Driven Fault-Fracture Meshes (JSG, 18, 1031).
Sierra, J.L., Pedro, G., D'Amore, F., 1992. Reservoir characteristics of the vapour dominated geothermal field of Copahue, Neuquén, Argentina, as established by isotopic and geochemical techniques. International Atomic Energy Agency, Technical Document. 641, pp. 13–30.
Stern, C.R., López-Escobar, L., Moreno, H., Clavero, J., Naranjo, J.A., Parada, M.A., Skewes, M.A., 2007. Chilean volcanoes. In: Gibson, T.M.A.W. (Ed.), The Geology of Chile. The Geological Society of London, pp. 149–180.
Sveinbjörnsdóttir, Á.E., Arnórsson, S., Heinemeier, J., 2001. Isotopic and chemical characteristics of old "ice-age" groundwater, North Iceland. Water–Rock Interaction, Balkema, pp. 205–208.
Tamburello, G., Agusto, M., Caselli, A., Tassi, F., Vaselli, O., Calabrese, S., Rouwet, D., Capaccioni, B., Di Napoli, R., Cardellini, C., et al., 2015. Intense magmatic degassing through the lake of Copahue volcano, 2013–2014. J. Geophys. Res. Solid Earth 120, 6071–6084.
Tardani, D., Reich, M., Roulleau, E., Takahata, N., Sano, Y., Perez-Flores, P., Sanchez-Alfaro, P., Cembrano, J., Arancibia, G., 2016. Exploring the feedbacks between structure and hydrothermal fluid composition using helium, nitrogen and carbon isotopes in a long-lived intra-arc strike slip fault. Geochim. Cosmochim. Acta 184, 193–211.
Varekamp, J.C., Ouimette, A., Herman, S.W., Bermudez, A., Delpino, D., 2001. Hydrothermal element fluxes from Copahue, Argentina: a beehive volcano in turmoil. Geo 29 (11), 1059–1062.
Varekamp, J.C., Ouimette, A., Herman, S.W., Flynn, K.S., Bermudez, A., Delpino, D., 2009. Naturally acid waters from Copahue volcano, Argentina, Appl. Geochemistry 24 (2), 208–220.
Velez, M.L., Euillades, P., Caselli, A., Blanco, M., Diaz, J.M., 2011. Deformation of Copahue volcano: inversion of InSAR data using a genetic algorithm. J. Volc. Geotherm. Res. 202 (1–2), 117–126.
Wibberley, C.A.J., Yielding, G., Di Toro, G., 2008. Recent advances in the understanding of fault zone internal structure: a review. Geol. Soc. Lond. Spec. Publ. 299 (1), 5–33.
Zlotnicki, J., Sasai, Y., Toutain, J.P., Villacorte, E.U., Bernard, A., Sabit, J.P., Gordon Jr., J.M., Corpuz, E.G., Harada, M., Punongbayan, J.T., Hase, H., Nagao, T., 2009. Combined electromagnetic, geochemical and thermal surveys of Taal volcano (Philippines) during the period 2005– 2006. Bull. Volcanol. 71:29–47. http://dx.doi.org/10.1007/s00445-008-0205-2.